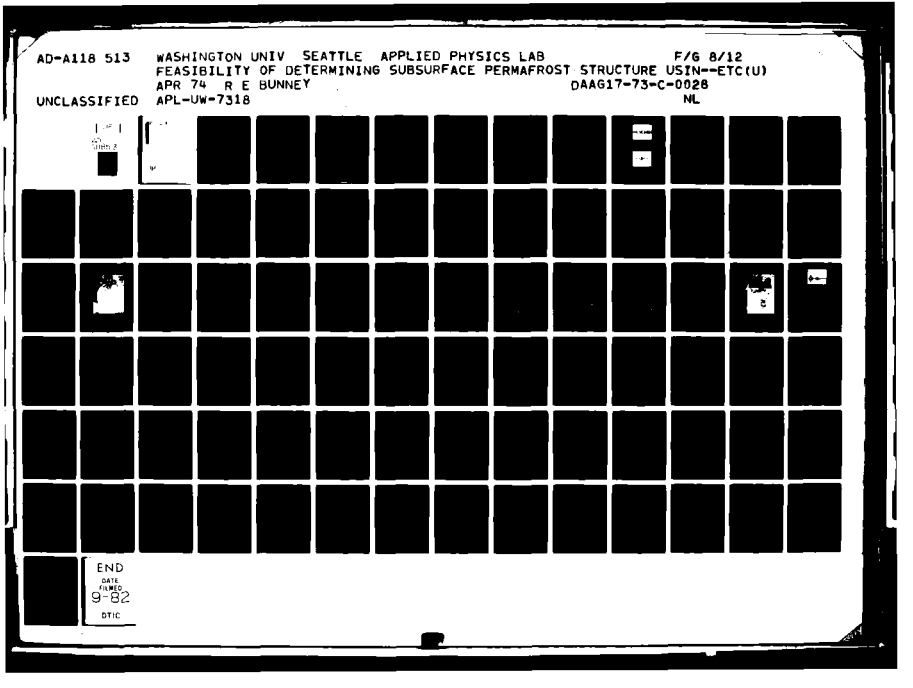
AD-A118 513
WASHINGTON UNIV SEATTLE APPLIED PHYSICS LAB F/G 8/12
FEASIBILITY OF DETERMINING SUBSURFACE PERMAFROST STRUCTURE USIN--ETC(U)
APR 74 R E BUNNEY DAAG17-73-C-0028
UNCLASSIFIED APL-UW-7318 NL
END
DATE FILMED
9-82
DTIC

APPLIED • PHYSICS • LABORATOR

A DIVISION OF THE UNIVERSITY OF WASHINGTO

# FEASIBILITY OF DETERMINING SUBSURFACE PERMAFROST STRUCTURE USING ACOUSTIC PULSE ECHO TECHNIQUES

by Robert E. Bunney

APL-UW 7318
JUNE 1974







CONTRACT DAAG17-73-C-0028

# FOREWORD

The investigation described herein was performed by Dr. R. E. Bunney, Division of Marine Resources, University of Washington, under Contract No. DAAG 17-73-C-0028 for the U.S. Army Cold Regions Research and Engineering Laboratory, sponsored by the Advanced Research Project Agency under ARPA Order 2096.

This contract was technically monitored by Dr. Y. Nakano, U.S. Army Cold Regions Research and Engineering Laboratory under the instruction of Commander J. R. Seesholtz, Program Manager, ARPA.

# CONTENTS

## SUMMARY

The principal object of this experiment was to evaluate the feasibility of using acoustic pulse echo techniques to determine the subsurface structure of permafrost. Laboratory tests performed on representative samples of permafrost, i.e., Ottawa sand, Hanover silt and Goodrich clay, show that such acoustic methods are reasonable, provided the acoustic wavelengths are long compared to the radius of the scattering centers and to the transition regions between adjacent constituents (e.g., sand, silt, clay, ice) of the permafrost.

Our velocity measurements showed that either previous measurements have been significantly high or the saturation levels of our samples were lower than anticipated. The test sections deteriorated visibly during the experimentation process. There was obviously dehydration due to sublimation of the surface moisture, but the extent of dehydration in the interior of the sample is not known. The velocity measurements suggest saturation levels of 35-40%.

Acoustic attenuation measurements were performed and the results are compared with scattering theory. The additional attenuation expected from dissipative processes is discussed but could not be evaluated because the dimensions of our samples were not large enough to allow the long wavelength tests necessary to determine the parameters required in the theory. The results of the tests did indicate, however, that if significant depth is to be obtained frequencies of less than 10 kHz must be utilized. It is also clear that an efficient method of coupling the energy into the medium must be investigated. From the results of our theories and measurements, there appears to be no significant difference between using the compressional and using the transverse acoustic mode.

The reflectivity at permafrost-ice interfaces was investigated and the results are compared with theory. Although both the predicted and measured losses in the reflected wave are appreciable, they do not appear to preclude using acoustic pulse echo techniques, provided the wavelengths are long enough to reduce the attenuation to acceptable levels. Extension of the theory to include transition layers between constituents of the medium is also discussed.

# INTRODUCTION

Many operations in arctic regions require detailed analysis of the shallow (<50 ft) permafrost subsurface. This information is particularly important, for example, in the construction of oil pipelines; in such cases, however, the survey of the permafrost subsurface should not only be efficient and not too costly but should have a minimal environmental impact. Determining the feasibility of using acoustic pulse echo methods to locate, and possibly evaluate, boundaries and discontinuities in the permafrost has been the subject of the study reported here.

The ability to use acoustic ranging to locate inclusions and discontinuities in permafrost formed by dry frost regions, the subpermafrost boundary, refrozen regions and/or upcroppings of base rock (all of which may serve as foundations for substantial structures) or to locate ice lenses, taliks, etc. (which can not) is dependent upon the acoustic properties of the respective media and the transition zones between them. Specifically, the densities and either the longitudinal and transverse acoustic velocities or the elastic moduli of the permafrost constituents must be very well known to determine the reflectivity at the interfaces; the attenuation as a function of frequency must also be known to determine the depth to which the method will be reliable.

A great deal of work has been done on measuring the velocity of sound in permafrost using seismic techniques (see the review by Barnes[1] and Zykov[2]). Hunter[3] has recently applied seismic techniques to mapping subsurface structures and has also reported the results of in situ compressional and transverse wave velocity measurements. Although laboratory measurements of the acoustic velocity in various constituents of permafrost have been performed for some time[4-6] and many theories[7-13] that are applicable to the propagation of sound in permafrost have been set forth, only in the last few years has significant progress been reported on determining the sound propagation properties of frozen soils. Kaplar[14] used a resonant method to determine the elastic moduli of several representative samples of permafrost and ice as a function of temperature. Timur[15] discusses the compressional velocity in terms of the ice-water-air constituents of the media and relates the observed increase in velocity to the cementation of the sand grains with ice. He also observed a hysteresis effect in the velocity coinciding with the freeze-thaw cycle and related it to interfacial forces and a slight salinity of the interstitial liquids. Nakano and his co-workers[16-18] have performed a series of careful laboratory experiments on samples of Ottawa sand, Goodrich clay and Hanover silt, measuring the compressional velocity using pulse echo techniques and measuring the shear velocity using Snell's law of critical angle methods. For the case of Ottawa sand, the velocity was related not only to temperature, where the hysteresis effect of Timur was observed, but also to the saturation of the sample.

As discussed previously, the attenuation of the sound as a function of frequency must be well known if the investigator is to maximize both the depth of penetration into the medium and the resolution with which the subsurface inclusions and discontinuities are observed. Unlike velocity, there unfortunately appears to have been little work performed in this area, at least in the laboratory. Anomalously high attenuation has been observed by Hunter[3] and by Press and Dobrin[19] during seismic experiments in regions of thin permafrost. However, since Donato[20] has shown that for this condition the attenuation is related to the ratio of the wavelength to the thickness of the sample, this anomaly is probably related to Lamb-like propagation modes[21] in the medium rather than its gross properties. An excellent review article (with extensive bibliography) on the attenuation of acoustic waves at seismic frequencies has been written by Jackson and Anderson.[22] However, because of the long wavelengths used in seismic work, the results in those studies may not be applicable to the problem being studied here because of the resolution that is required to adequately analyze the subsurface structure.

# EXPERIMENTS

## Samples

The data reported were obtained on idealized, i.e., homogeneous and isotropic, samples of representative permafrost constituents furnished by the U.S. Corps of Engineers' Cold Regions Research and Engineering Laboratory. Specifically, we used samples of 20-30 Ottawa sand, Hanover silt and Goodrich clay, formed in cylinders approximately 6 inches in diameter and 18 inches long. To prepare the samples, the dry soil was saturated with distilled water, and then placed in a mold. The mold was placed in a cold room and subjected to rotary motion to prevent localized concentrations due to gravity while the sample was freezing.[17]

During the course of the experiment, some evidence of deterioration became apparent. Cross sections of the sample indicate this deterioration certainly was caused by sublimation at the surface and perhaps contributed to a general degeneration of the sample. It most assuredly was a contributing factor to the anomalous results that are discussed later.

## Results of Velocity Measurements

Figure 1 is a block diagram of the instrumentation used to obtain the velocity, attenuation and reflectivity measurements. In this system a pulse timing generator furnishes pulse length and rate information to a pulsed power oscillator, and a trigger signal to the oscilloscope. The oscillator, in turn, provides a cw pulse of the desired frequency, rate and length to an acoustic transducer coupled to the sample. The transmitted acoustic signal is received by a second transducer fixed to the opposite side of the test section, amplified, and transmitted to the oscilloscope.

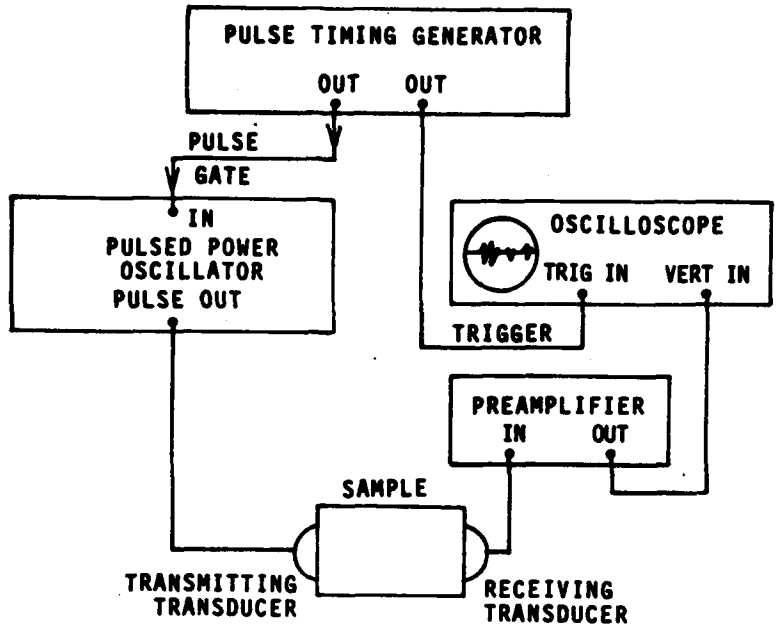


*Figure 1. Block diagram of instrumentation.*

The time of flight of the acoustic pulse in the sample is determined by measuring, with a calibrated time delay, the oscilloscope sweep time from the origin to the first received signal and to the subsequent arrivals that represent multiple reflections in the test section. Typical results are shown in Figures 2 and 3.

On relatively homogeneous materials, measurements using this technique are normally accurate to within 1 1/2%, with the largest error in the measurement of length. For the materials being discussed here, however, the velocity measurements are not that accurate because of loss of resolution due to multipath spreading of the pulse during transmissions and, in some cases, because of the long wavelengths required due to the high attenuation.

The results of the velocity measurements are shown in Figures 4-6 and the mean values are tabulated in Table I. During the tests, the sample temperature was maintained as nearly constant as possible at -15°C.

*Table I. Tabulation of average velocities.*

| Material | Ottawa Sand | Hanover Silt | Goodrich Clay |
|---|---|---|---|
| Comp. Vel. | 3417 ± 435 m/sec | 3096 ± 309 m/sec | |
| Trans. Vel. | 2266 ± 424 m/sec | 1805 ± 333 m/sec | 2065 ± 206 m/sec |

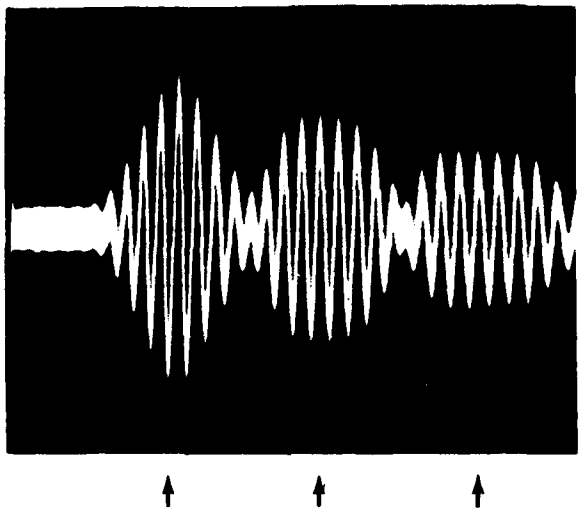

*Figure 2. Typical result of velocity experiment on Ottawa sand. Frequency = 64 kHz, sweep = 50 μsec/cm.*

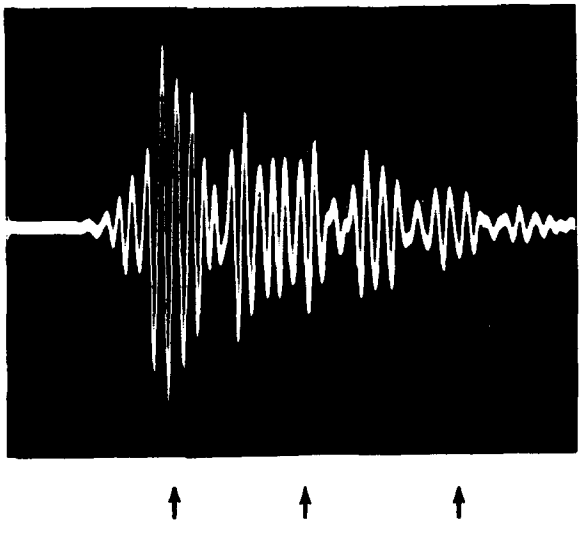

*Figure 3. Typical result of velocity experiment on Hanover silt. Frequency = 82 kHz, sweep = 50 μsec/cm.*

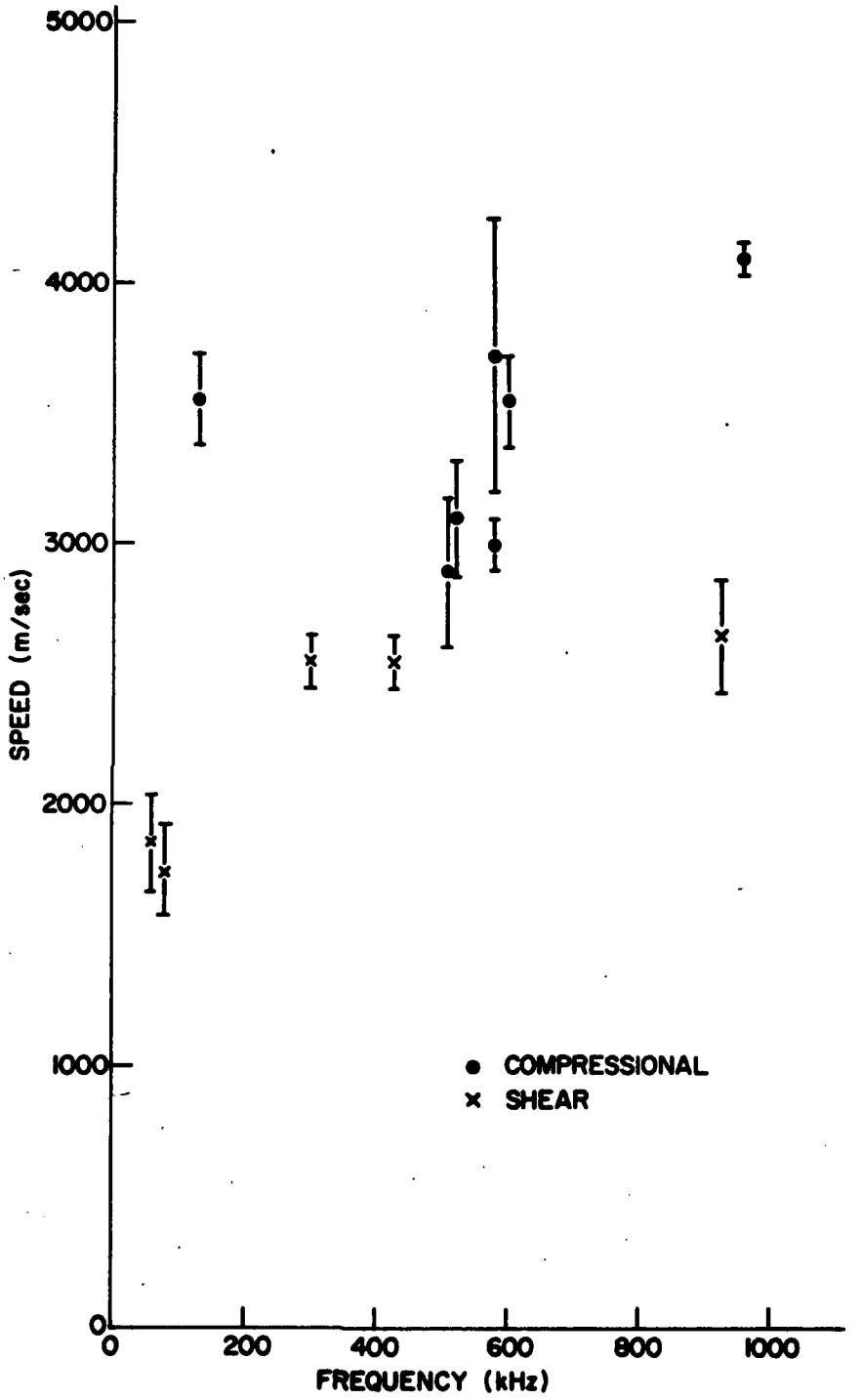


*Figure 4. Velocity vs frequency, Ottawa sand.*

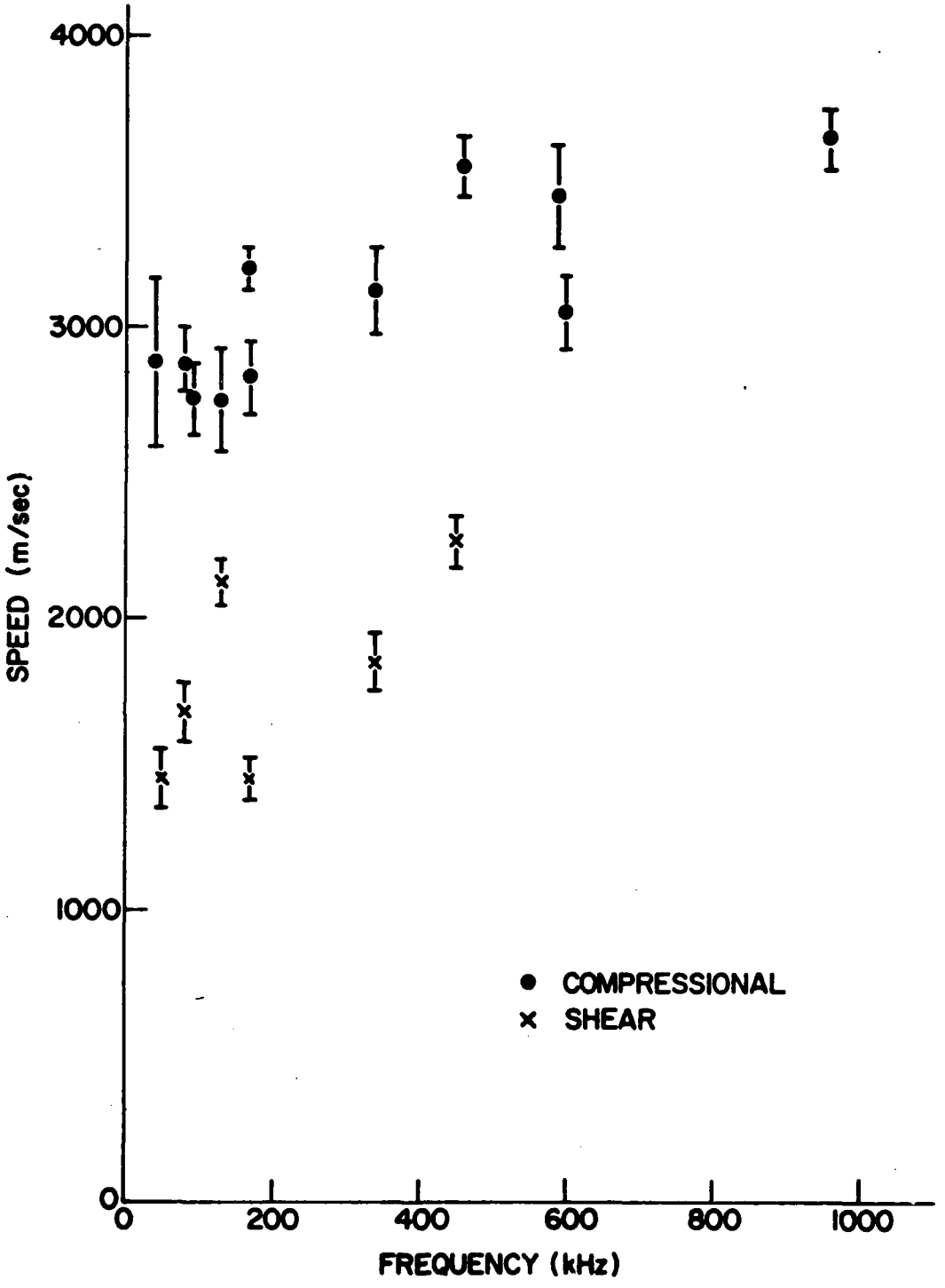


*Figure 5. Velocity vs frequency, Hanover silt.*

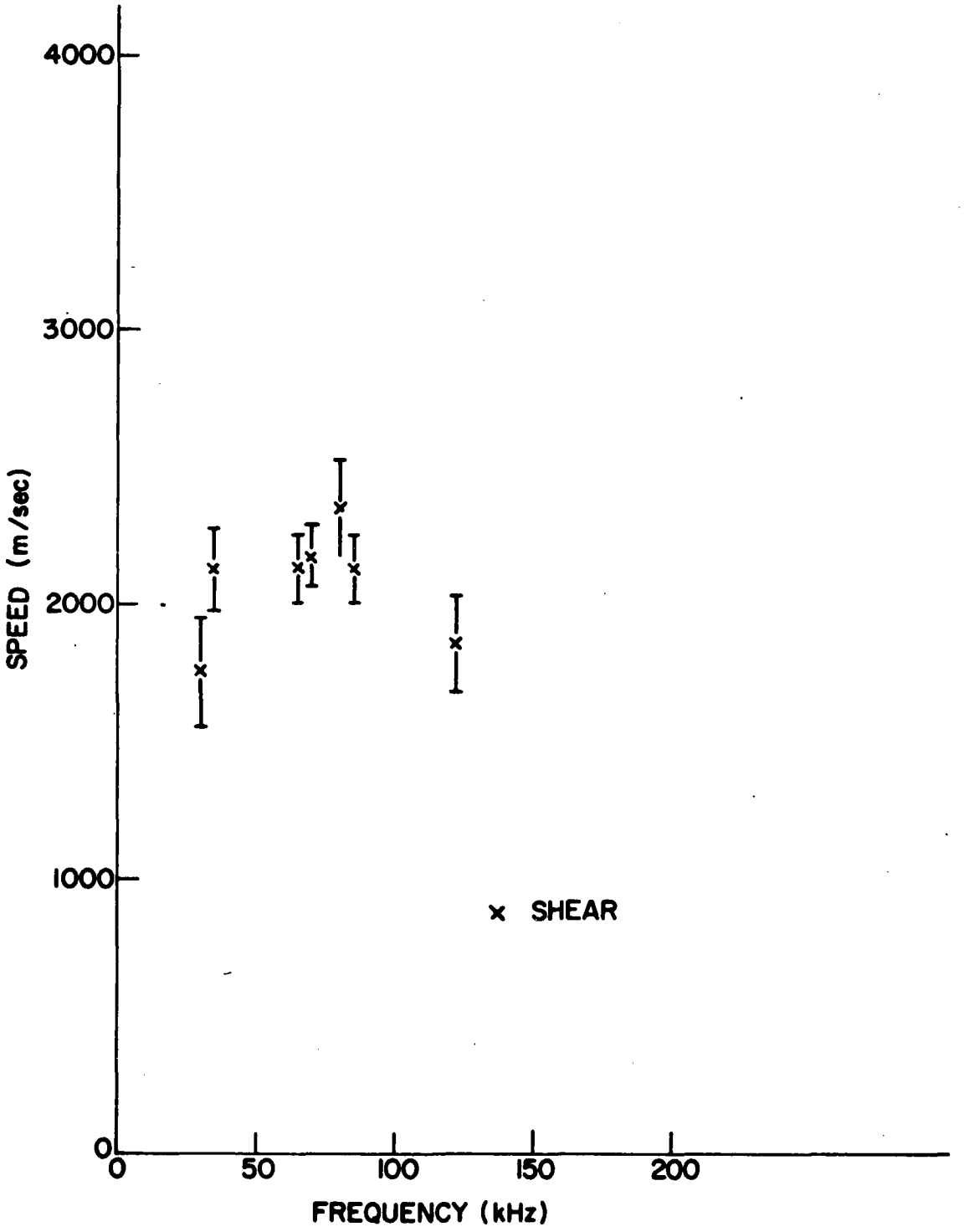


*Figure 6. Velocity vs frequency, Goodrich clay.*

The results differ appreciably from those of Nakano and Froula[18] (Figures 7 and 8) at the same temperature. Although the cause of the disparities is not known, dehydration of the samples is a strong possibility. This hypothesis is substantiated by Nakano's and Arnold's[17] measurements of the velocity in frozen Ottawa sand vs saturation and temperature (see Figures 9 and 10, and Table II). These data indicate that our Ottawa sand samples, rather than being totally saturated, actually were only saturated to 35-40%. Unfortunately, similar data are unavailable for Hanover silt and Goodrich clay. These materials would be expected, however, to behave in a fashion similar to that of Ottawa sand. Thus, the lower velocity values observed, particularly in the case of Hanover silt, are probably due to a lower saturation level and are not necessarily surprising.

*Table II. Description of Specimens*

| Specimen | Thickness d (cm) | Wet Density ($g/cm^3$) | Dry Density ($g/cm^3$) | Water Content* (%) | Void Ratio | Ice Saturation† (%) |
|---|---|---|---|---|---|---|
| 1 | 2.394 | 1.962 | 1.609 | 21.91 | 0.6470 | 99.70 |
| 2 | 2.373 | 1.863 | 1.598 | 16.59 | 0.6583 | 74.19 |
| 3 | 2.437 | 1.773 | 1.554 | 14.09 | 0.7053 | 58.82 |
| 4 | 2.399 | 1.771 | 1.589 | 11.47 | 0.6677 | 50.57 |
| 5 | 2.363 | 1.715 | 1.565 | 9.59 | 0.6933 | 40.72 |
| 6 | 2.400 | 1.717 | 1.592 | 7.85 | 0.6646 | 34.77 |
| 7 | 1.321 | 1.670 | 1.590 | 5.04 | 0.6667 | 22.27 |
| 8 | 1.339 | 1.604 | 1.562 | 2.66 | 0.6965 | 11.24 |
| 9 | 1.318 | 1.588 | 1.572 | 1.02 | 0.6858 | 4.40 |
| 10 | 1.311 | 1.580 | 1.580 | 0.00 | 0.6772 | 0.00 |

*Weight percent of water referred to the unit weight of dry soil.

†Weight percent of ice referred to the weight of ice, which could fill total void. (after Nakano and Arnold[17])

## Results of Attenuation Measurements

The attenuation of the acoustic wave in the medium is a principal concern in determining both the resolution and depth that can be attained with pulse echo techniques. This attenuation, whether originating from dissipative considerations (i.e., internal friction, thermal dissipation, viscous slippage at crystal boundaries, etc.) or from acoustic scattering from inhomogeneities in the medium, is very sensitive to frequency. In fact, the resolution of the technique is inversely proportional to the frequency of the acoustic wave. Thus to optimize his experiments, the investigator must be able to predict the attenuation as a function of frequency.

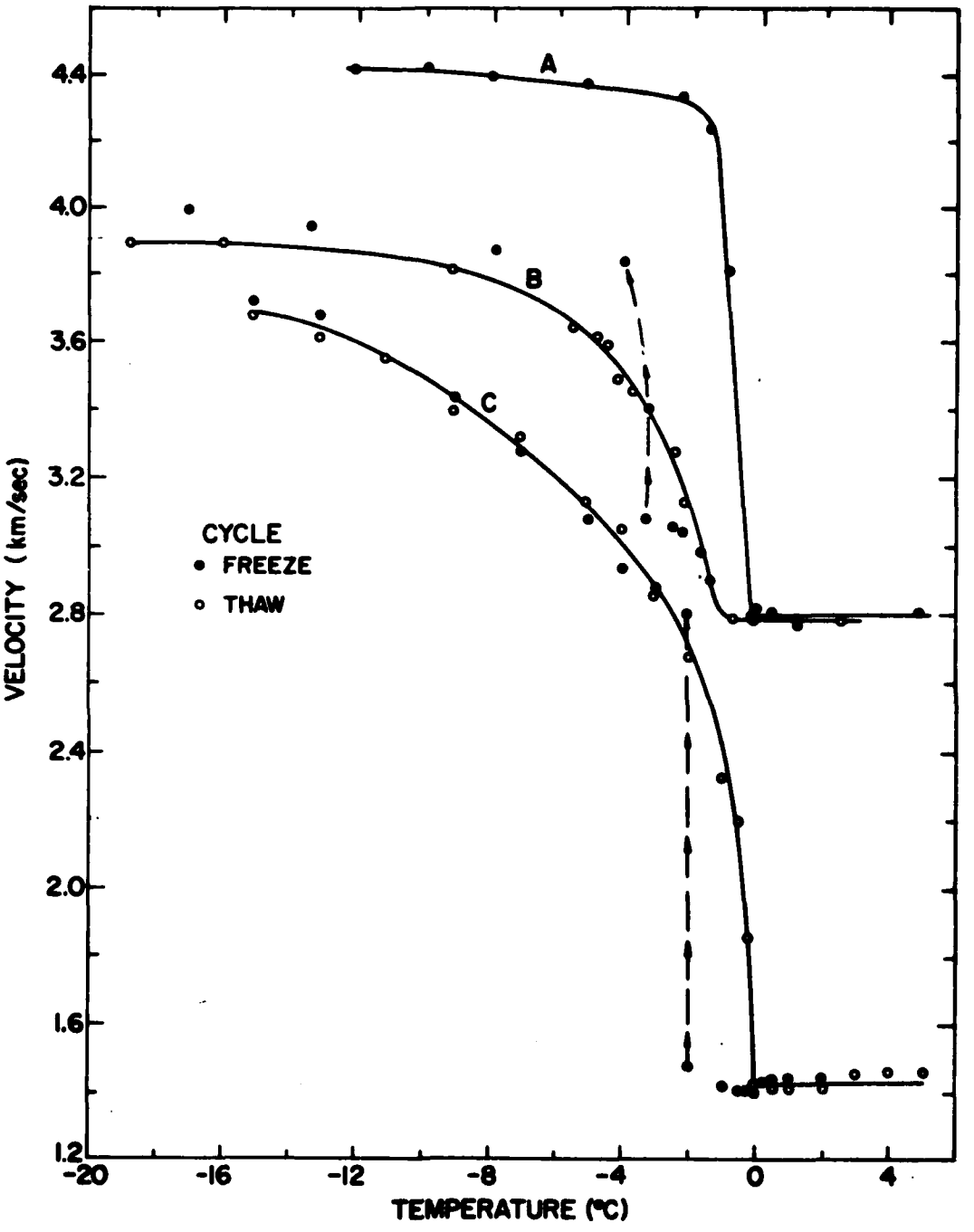


*Figure 7. The dilatational wave velocity vs temperature for: A) 20-30 Ottawa sand, wet density ρ = 2.20 g/cm³, B) Hanover silt, ρ = 1.83 g/cm³, and C) Goodrich clay, ρ = 1.80 g/cm³ under fully water-saturated conditions. Notice the discrepancy between the freezing and thawing cycles for B and C. No discrepancy was observed for Ottawa sand.* (after Nakano[18])

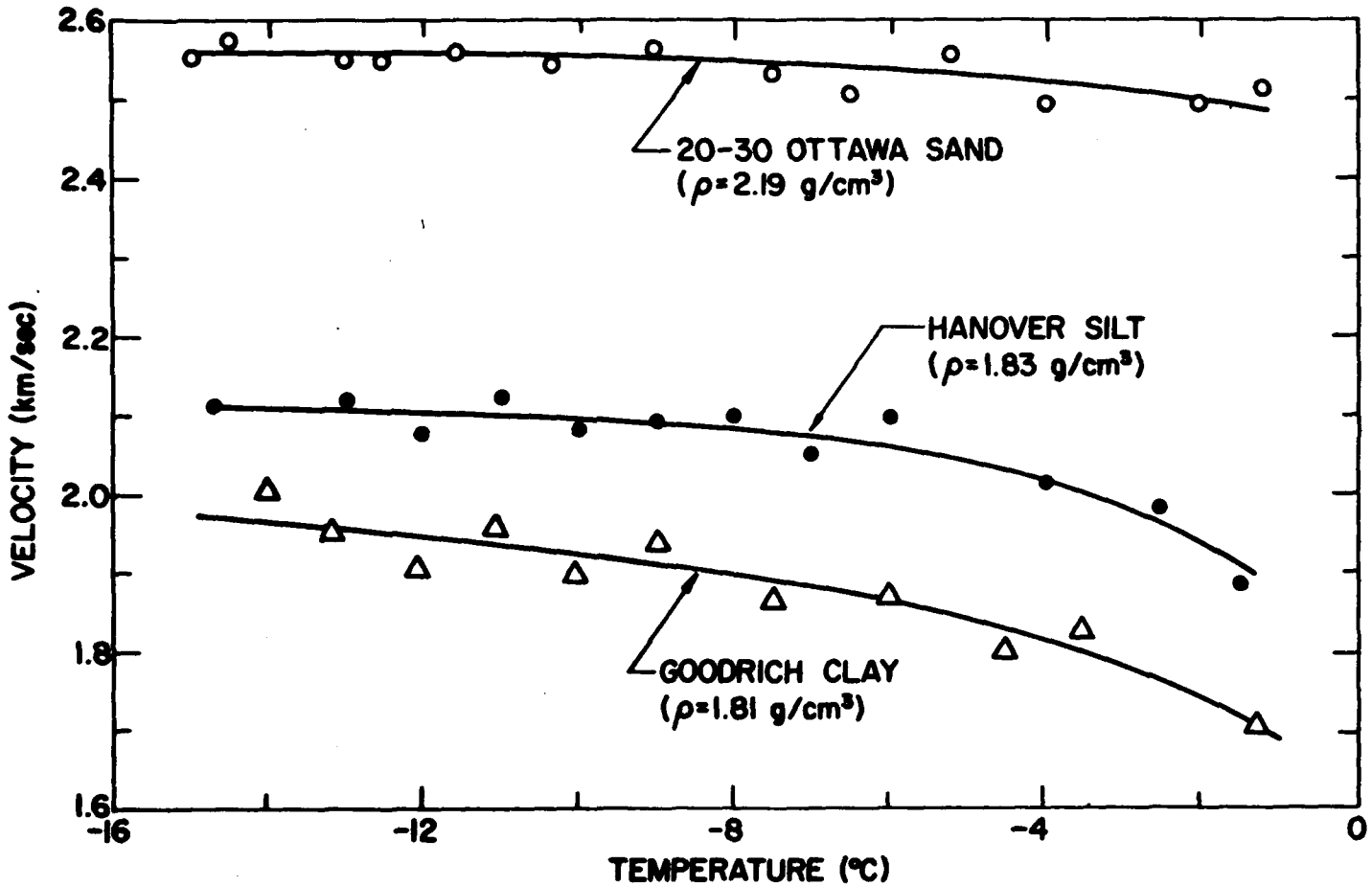


*Figure 8. The shear wave velocity versus temperature for 20-30 Ottawa sand, Hanover silt, and Goodrich clay under fully water-saturated conditions. Wet density is ρ.* (after Nakano[18])

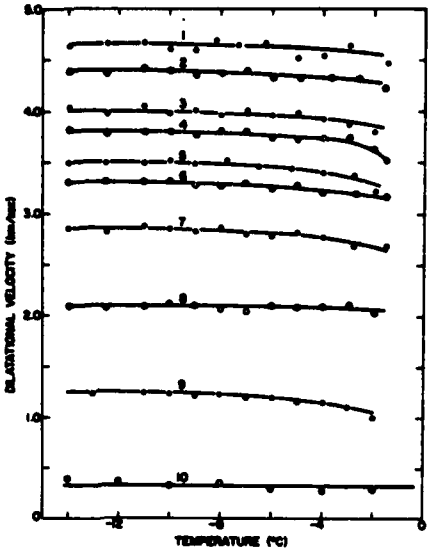


*Figure 9. Dilatational wave velocity versus temperature under various conditions of ice saturation. The number assigned to each curve corresponds to the specimen number.* (after Nakano and Arnold[17])

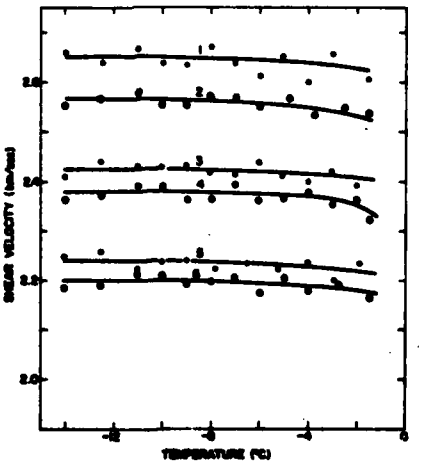


*Figure 10. Shear wave velocity versus temperature under various conditions of ice saturation. The number assigned to each curve corresponds to the specimen number.* (after Nakano and Arnold[17])

An acoustic wave propagating in a nonhomogeneous medium will interact with the inhomogeneities and part of the energy will be scattered out of the sound beam. When the wavelength of the sound is large compared to the size of these scattering centers, the interaction is minimal and the energy loss is small compared to that caused by classical dissipation. For this situation, the acoustic attenuation can be predicted by the long wavelength theories discussed in Appendix A. However, when the size of the scattering center is a significant portion of the wavelength, the attenuation due to scattering cannot be neglected.

To determine the attenuation due to scattering, consider an isotropic solid elastic medium containing a concentration of scatterers. The inhomogeneities in the medium can be mathematically characterized by a generalized function,

$$D(S,I,a,\vec{r}\ldots) = S(s_i)I(s_i,s_j)G(a,\vec{r}) \ldots, \tag{1}$$

where $S(s_i)$ is a structure distribution function which describes the relative importance of the various types of scatterers in the medium, $I(s_i,s_j)$ is a distribution function which describes the interaction between scatterers and multiple scattering of the sound, and $G(a,\vec{r})$ describes the distribution of the size and position, etc. of the scatterers.

Assuming a plane wave moving in the positive x-direction, the intensity of the sound is given by

$$I = I_o\, e^{-2\alpha x}\ , \tag{2}$$

where $\alpha$ is the attenuation constant, x is the penetration distance into the material and $I_o$ is the intensity of the original sound wave. If the energy losses are all considered to be caused by scattering processes, Eq. (2) may be rewritten

$$I = I_o\, e^{-\Gamma x}\ , \tag{3}$$

where $\Gamma$ is the generalized scattering cross section and is governed by the size, shape, position, etc. of the scatterers in the medium. In terms of Eq. (1), $\Gamma$ may be written

$$\Gamma = \sum_{i,j} \int_{\vec{r}} \int_{a} \ldots D(S,I,G,\vec{r},\ldots)\ \gamma_i(a)\, d\vec{r}\, da \ldots\ , \tag{4}$$

where now $\gamma_i(a)$ is the scattering cross section of a single independent scatterer. The attenuation is then given by

$$\alpha = \frac{1}{2} \sum_{ij} \int_{\vec{r}} \int_{a} \ldots D(S,I,G,\vec{r},\ldots)\ \gamma_i(a)\, d\vec{r}\, da \ldots\ . \tag{5}$$

This equation states that the attenuation is determined by the scattering cross section and the distribution of the scatterers. The cross section is dependent upon the interaction of the wave with each individual scatterer, while the distribution function is the probability of the wave encountering that scatterer in the medium.

For purposes of calculation, permafrost is considered to be composed of an array of elastic scatterers, i.e., granules of Ottawa sand, etc., imbedded in an ice matrix. To calculate the scattering cross section of a single scatterer, the problem shown in Figure 11 must be resolved.

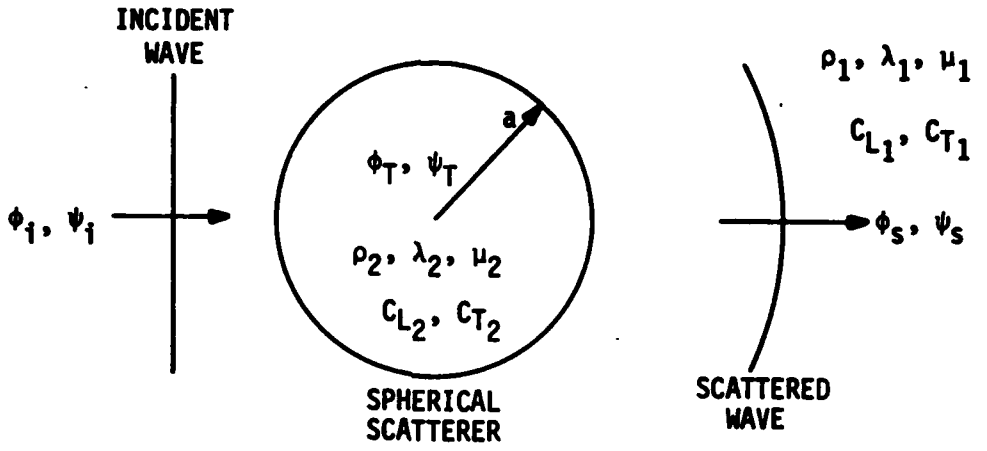


*Figure 11. Representation of the problem.*

Incorporating the methods of Ying and Truell[23] and of Corbato´ and Uretsky,[24] and using the experimentally measured values of velocity and density as reported by Nakano,[18] the product of the scattering cross section and the square of the frequency ($\gamma\nu^2$) were calculated numerically as a function of the circumference-to-wavelength ratio for both a shear and compressional incident plane wave. The results of this calculation are shown in Figures 12-14. In the frequency region for ka<<1, i.e., for wavelengths much larger than the scatterer radius, the scattering cross section is of the form

$$\gamma \sim \nu^4 a^6 \ , \tag{6}$$

which is the result expected from standard Rayleigh[25] scattering. In general, the scattering cross sections for ka<1 and ka>15 can be approximated by

Goodrich clay

$$\gamma_{comp} = \frac{\nu^4 a^6}{4.19 \times 10^{-8}\ \nu^{3.5}\ a^{3.5} + 5.42 \times 10^{-9}} \ dB/cm^2$$

$$\gamma_{shear} = \frac{\nu^4 a^6}{5.36 \times 10^{-3}\ \nu^2\ a^2 + 4.84 \times 10^{-9}} \ dB/cm^2 \tag{7}$$

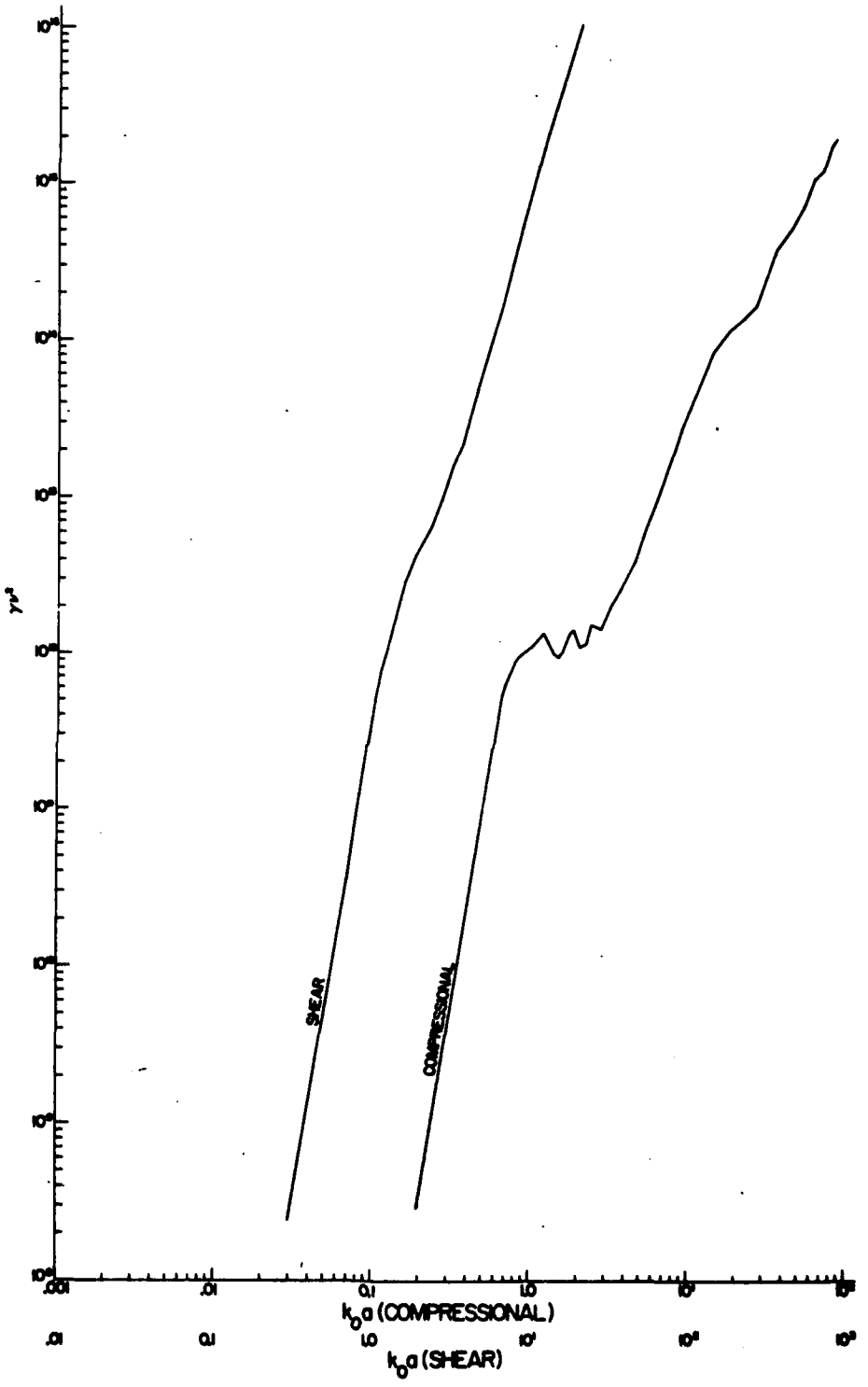


*Figure 12. Results of the cross section calculation for Ottawa sand.*

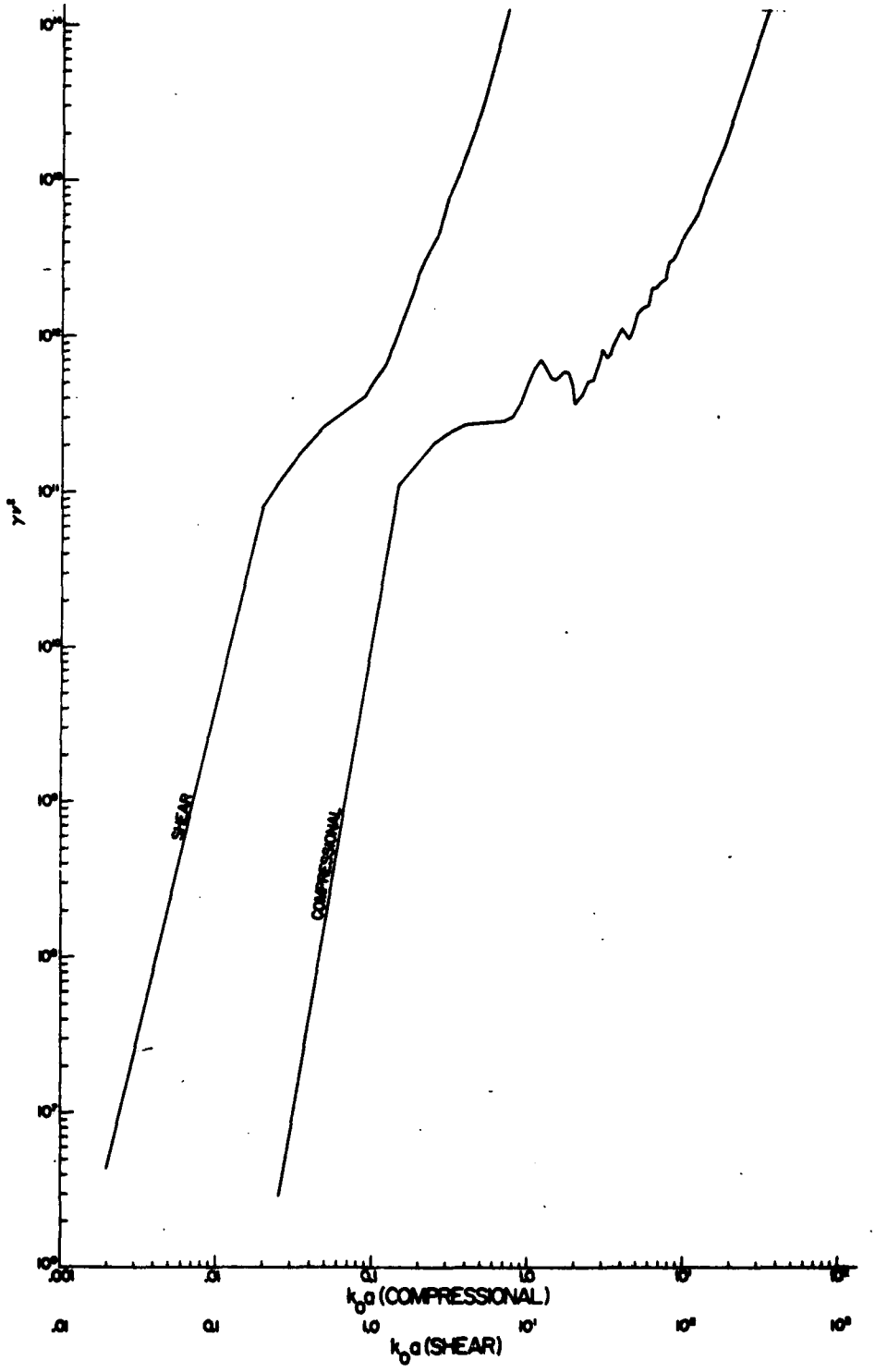


*Figure 13. Results of the cross section calculation for Hanover silt.*

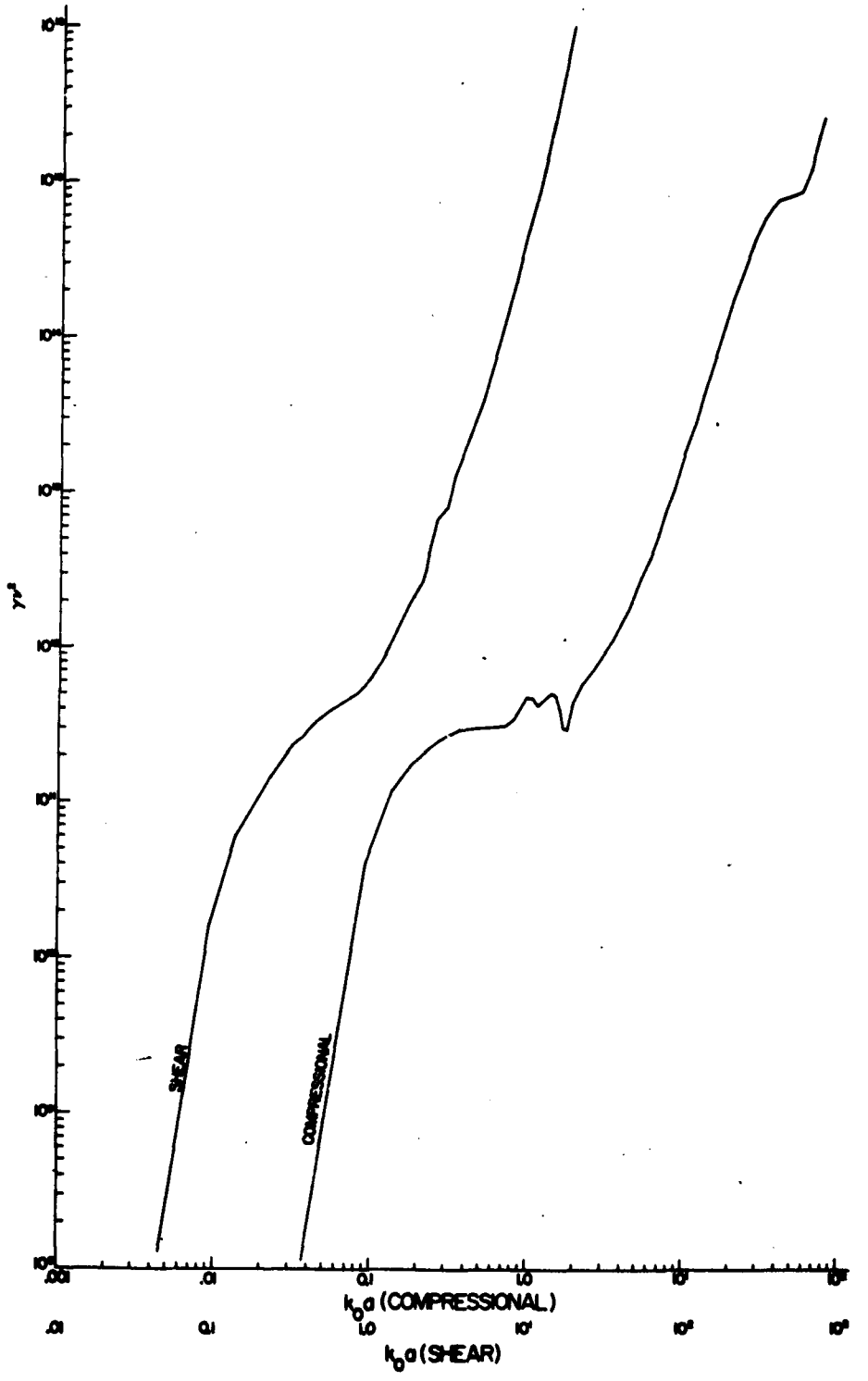


*Figure 14. Results of the cross section calculation for Goodrich clay.*

Hanover silt

$$\gamma_{comp} = \frac{\nu^4 a^6}{2.56 \times 10^{-1}\ \nu^3\ a^3 + 3.62 \times 10^{-12}}\ dB/cm^2$$

$$\gamma_{shear} = \frac{\nu^4 a^6}{2.17 \times 10^{-2}\ \nu^{2.44}\ a^{2.44} + 1.1242 \times 10^{-10}}\ dB/cm^2 \qquad (8)$$

Ottawa sand

$$\gamma_{comp} = \frac{\nu^4 a^6}{1.03 \times 10^{-11}\ \nu^{3.9}\ a^{3.9} + 4.75 \times 10^{-10}}\ dB/cm^2$$

$$\gamma_{shear} = \frac{\nu^4 a^6}{7.86 \times 10^{-9}\ \nu^{2.41}\ a^{2.41} + 6.87 \times 10^{-13}}\ dB/cm^2 \qquad (9)$$

where the frequency is in megahertz and the scatterer radius, a, is in centimeters.

To evaluate the attenuation due to scattering from these expressions, the distribution functions in the medium must be either known or assumed. Because the necessary data are presently unavailable, and to minimize the complexity of the calculation, the following assumptions have been made.

1. No interaction exists between the scattering centers, and the wave, once scattered, will not be re-scattered back into the sound beam. This approximation is not extremely valid for materials with as high a concentration of scattering centers as those being discussed here and will tend to make the predictions somewhat higher than if multiple scattering had been considered.

2. There are N scattering centers per unit volume and the centers are uniformly distributed throughout the medium. With the exception of the Goodrich clay sample, this appears to be a reasonable assumption. It will, of course, not be valid for in situ measurements.

3. All of the scattering centers are of the same size, with a radius $a_o$. Since the materials used in the manufacture of the test samples were filtered for size, this assumption is perfectly reasonable. During field tests, this assumption becomes invalid. However, if radius $a_o$ is selected as the average scatterer size, then it can be argued that only the larger

inhomogeneities in the distribution will affect the scattering. This assumption will make the calculated attenuation less than that expected during the experiment.

Using, these assumptions, the attenuation due to scattering may be written

$$\alpha_{scattering} = \frac{N}{2} \gamma(a_o) \ , \tag{10}$$

which predicts the "first order" attenuation to be expected from the scattering mechanism. Using the curves of Figures 12 through 14 and the relation

$$ka = \frac{2\pi\nu}{C} a \ , \tag{11}$$

where $\nu$ is the frequency in hertz, C is the velocity in centimeters per second, and a is the radius of the scatterers in centimeters, the attenuation due to scattering for values ka<1 and ka>15 can be approximated by:

Ottawa sand

$$\alpha_{comp} = \frac{\nu^4}{1.14 \times 10^{-2} \nu^{3.9} + 1.44 \times 10^{-6}} \text{ dB/m}$$

$$\alpha_{shear} = \frac{\nu^4}{6.52 \times 10^{-3} \nu^{2.41} + 2.086 \times 10^{-7}} \text{ dB/m} \tag{12}$$

Hanover silt

$$\alpha_{comp} = \frac{\nu^4}{5.12 \times 10^{-3} \nu^3 + 4.63 \times 10^{-9}} \text{ dB/m}$$

$$\alpha_{shear} = \frac{\nu^4}{3.42 \times 10^{-3} + 1.44 \times 10^{-7}} \text{ dB/m} \tag{13}$$

Goodrich clay

$$\alpha_{comp} = \frac{\nu^4}{5.50 \times 10^{-2} \nu^{3.5} + 1.15 \times 10^{-5}} \text{ dB/m}$$

$$\alpha_{shear} = \frac{\nu^4}{1.14 \times 10^{-2} \nu^2 + 1.03 \times 10^{-6}} \text{ dB/m} \tag{14}$$

where $\nu$ is in megahertz. For values of $1 < ka < 15$, the approximations of Eqs. (12) through (14) are still more or less valid for order of magnitude calculations, but will invariably yield predictions that are significantly low.

Equations (12) through (14) have been solved as a function of frequency and the solutions are shown in Figures 15 through 17. For the frequencies considered during these experiments, relatively good agreement was observed between the theory and the experiment, with the exception of the Goodrich clay samples. The reason for the variance between the theory and the results of the Goodrich clay experiment can be seen in Figure 18. The theories assume both total saturation and homogeneity. Earlier it was speculated that during the course of the experiment the test samples degenerated appreciably because of dehydration. This degeneration was assumed to be limited to sublimation of the surface areas, but subsequent analysis of the velocity data has shown that the samples were not totally saturated at the time of the experiment. Figure 18 indicates that homogeneity also was not necessarily achieved in the test samples.

At the beginning of this section we mentioned the attenuation loss due to dissipative mechanisms, i.e., thermal losses, internal friction, viscous slippage, etc. These processes have not been specifically evaluated for the permafrost specimens studied here, primarily because the dimensions of the test samples precluded using acoustic frequencies that were very long compared to the radius of the scattering centers. Further experimentation should be performed to acquire the long-wavelength parameters necessary to evaluate the long wavelength solutions discussed in Appendix A.

## Results of Reflectivity Measurements

The energy of an acoustic wave encountering a boundary between two elastic media is divided between reflected and transmitted modes (see Figure 19). To determine the feasibility of analyzing the subsurface structure of permafrost, the relative amount of energy in the reflected modes must be known. In Appendix A, the problem of two ideal elastic media in rigid contact, i.e., presuming no slippage at the boundary, has been solved as a function of incident angle for both compressional and transverse acoustic waves incident on a permafrost-to-ice boundary. The results of this calculation are shown in Figures 20-25 and indicate that, for normal incidence, a minimum loss of 7 to 11 dB is to be expected at the boundary, depending on the mode of the incident wave and the permafrost material; for an Ottawa sand-Goodrich clay interface (Figures 26 and 27), losses exceeding 13 dB can be anticipated in the reflected wave.

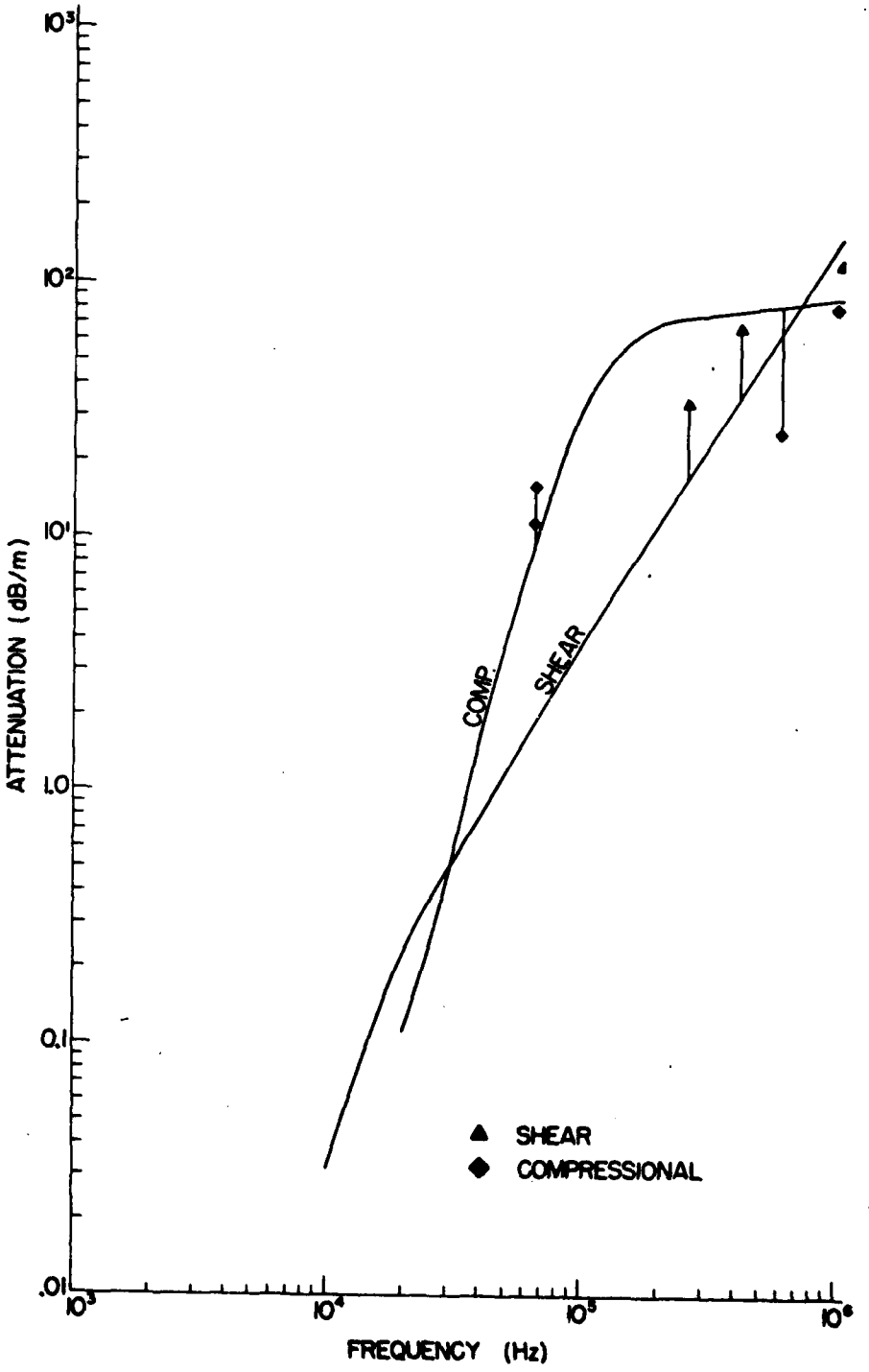


*Figure 15. Attenuation vs frequency (scattering only), Ottawa sand.*

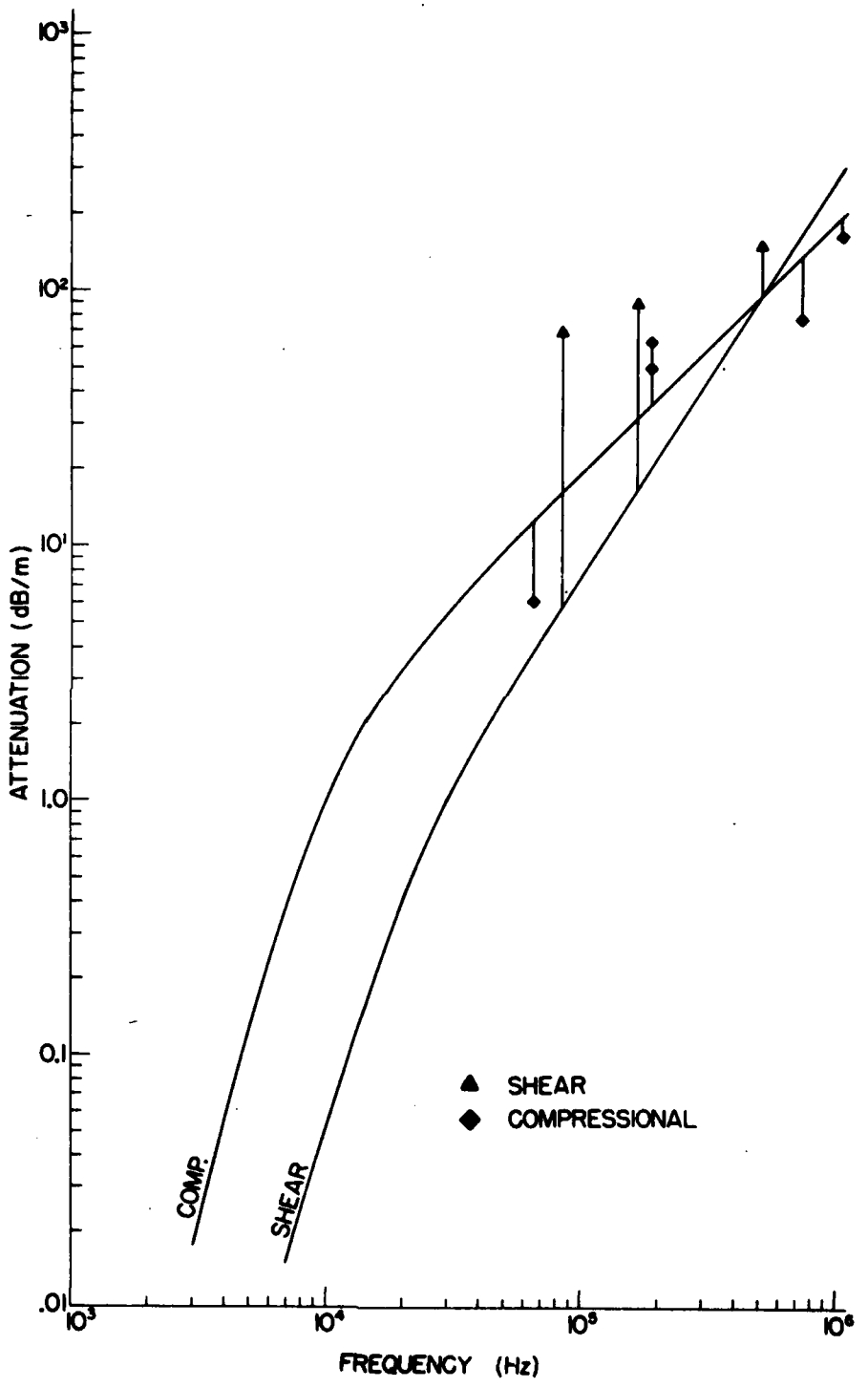


*Figure 16. Attenuation vs frequency (scattering only), Hanover silt.*

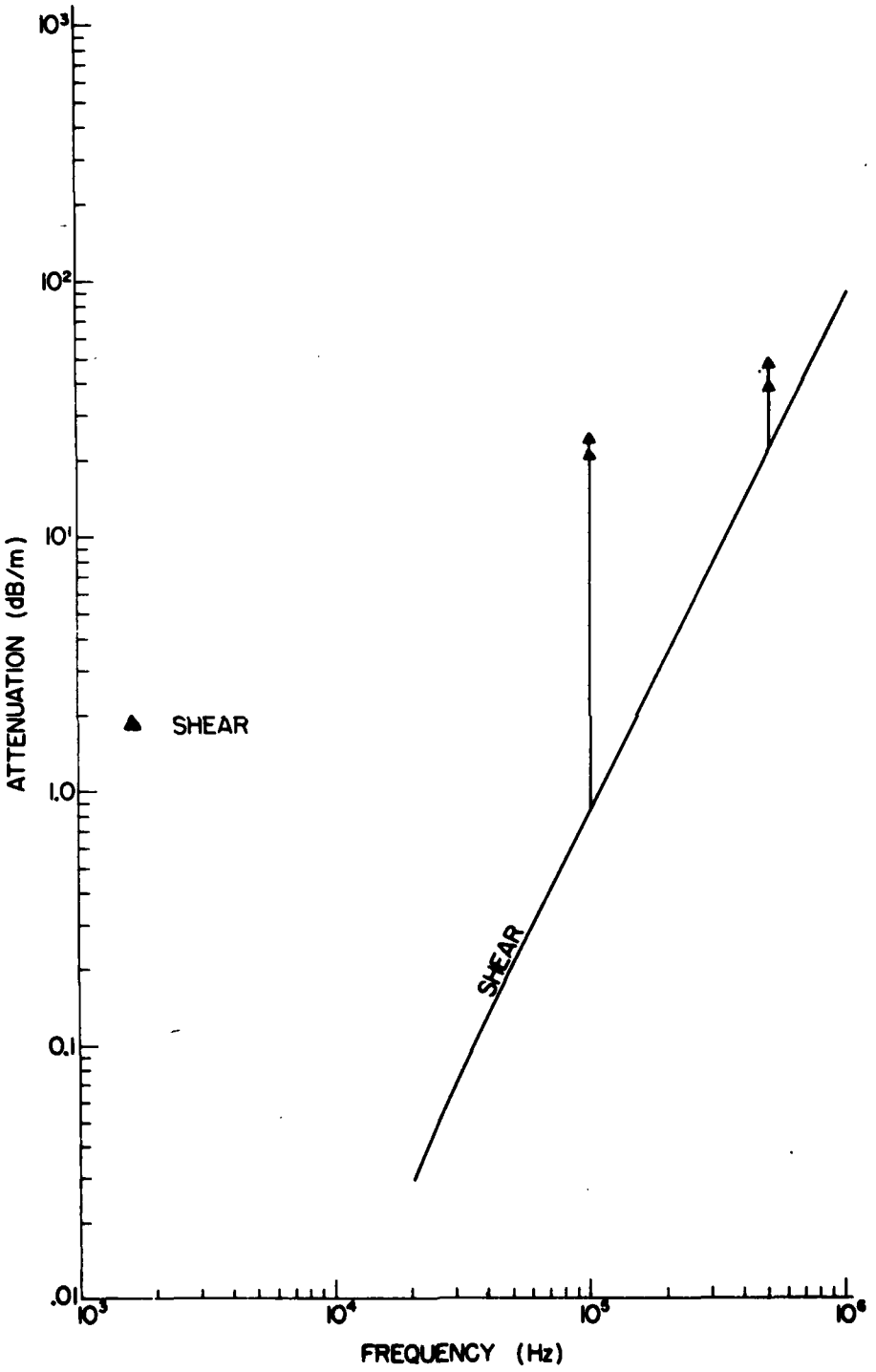


*Figure 17. Attenuation vs frequency (scattering only), Goodrich clay.*

*Figure 18. Photograph of cross section of Goodrich clay sample.*

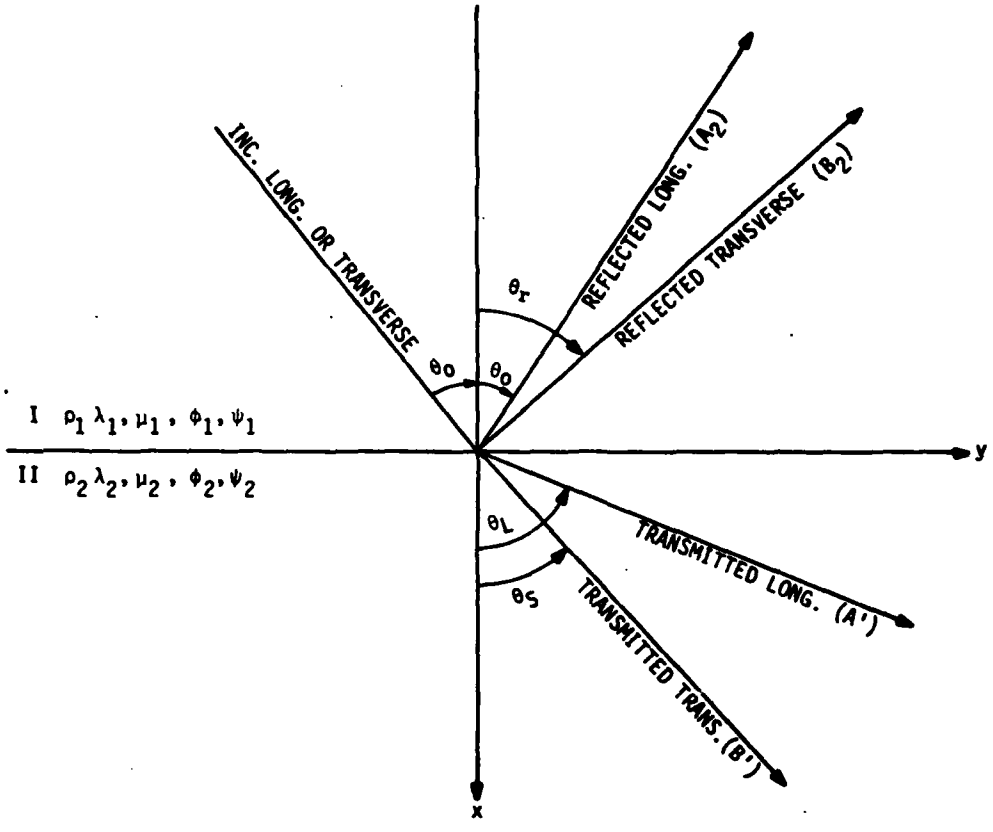


*Figure 19. Acoustic wave reflections and transmissions at an elastic interface.*

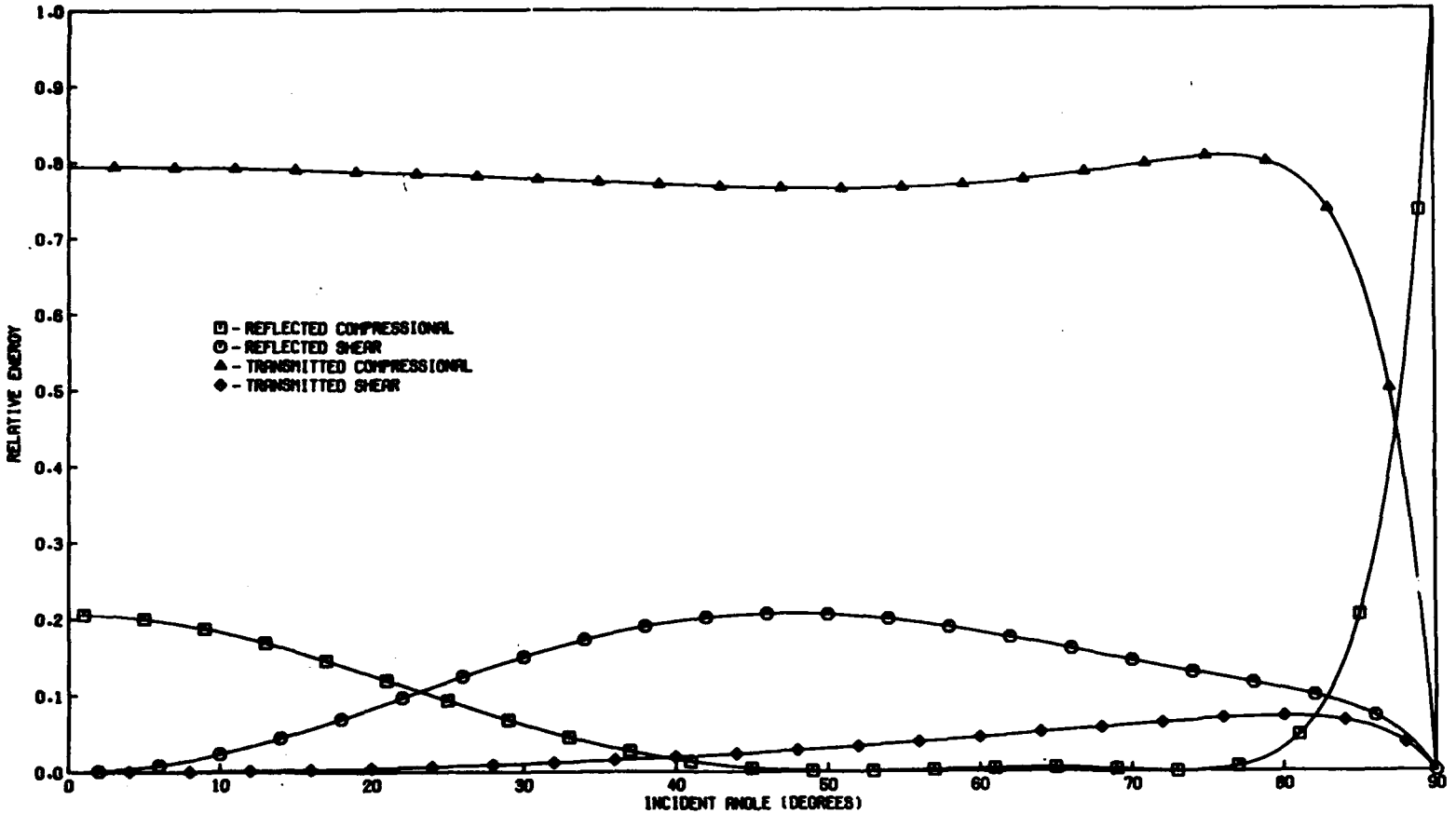


*Figure 20. Relative energy distribution of acoustic wave incident on permafrost-ice boundary, Ottawa sand-ice (compressional wave incident).*

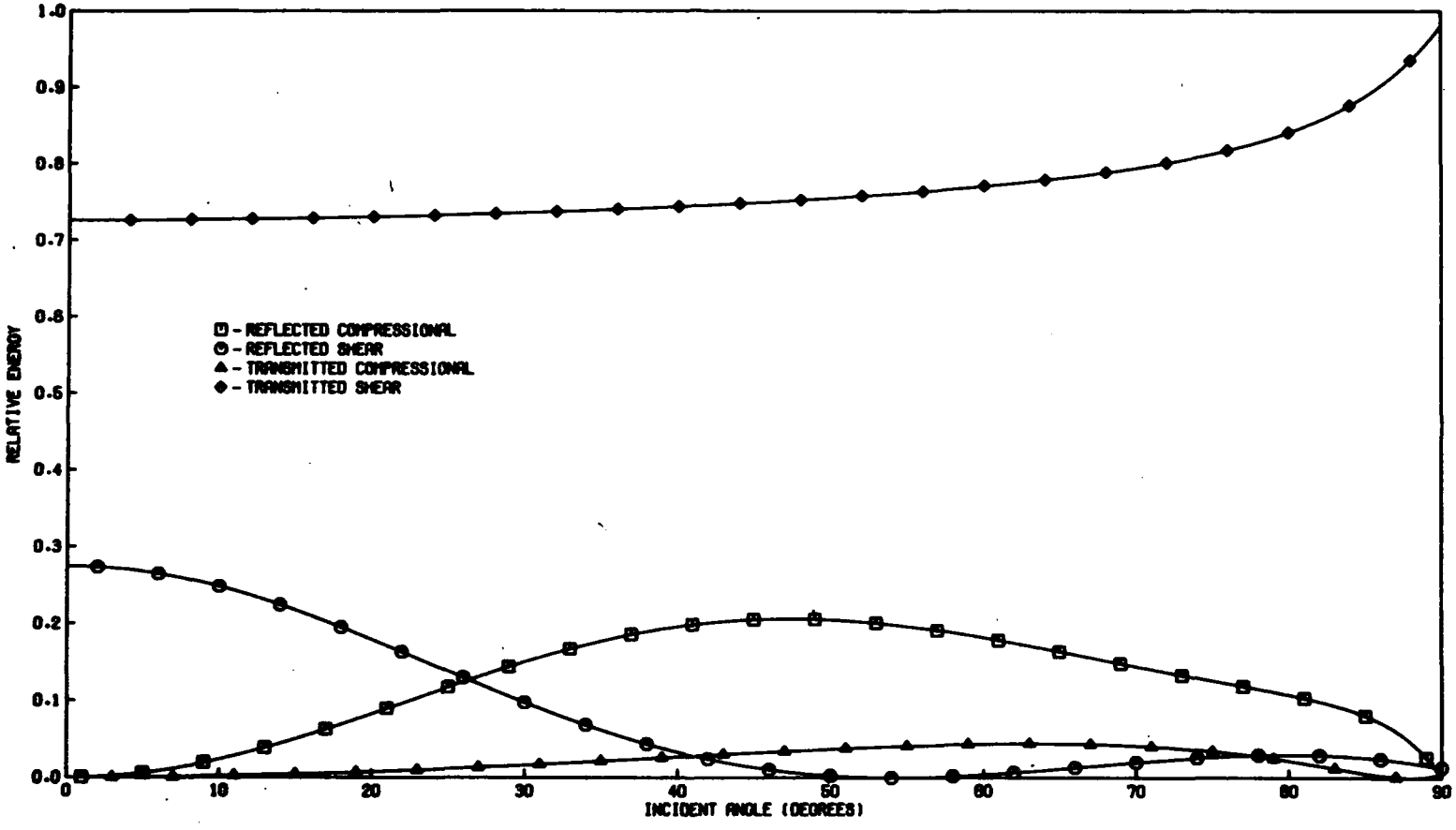


*Figure 21. Relative energy distribution of acoustic wave incident on permafrost-ice boundary, Ottawa sand-ice (transverse wave incident).*

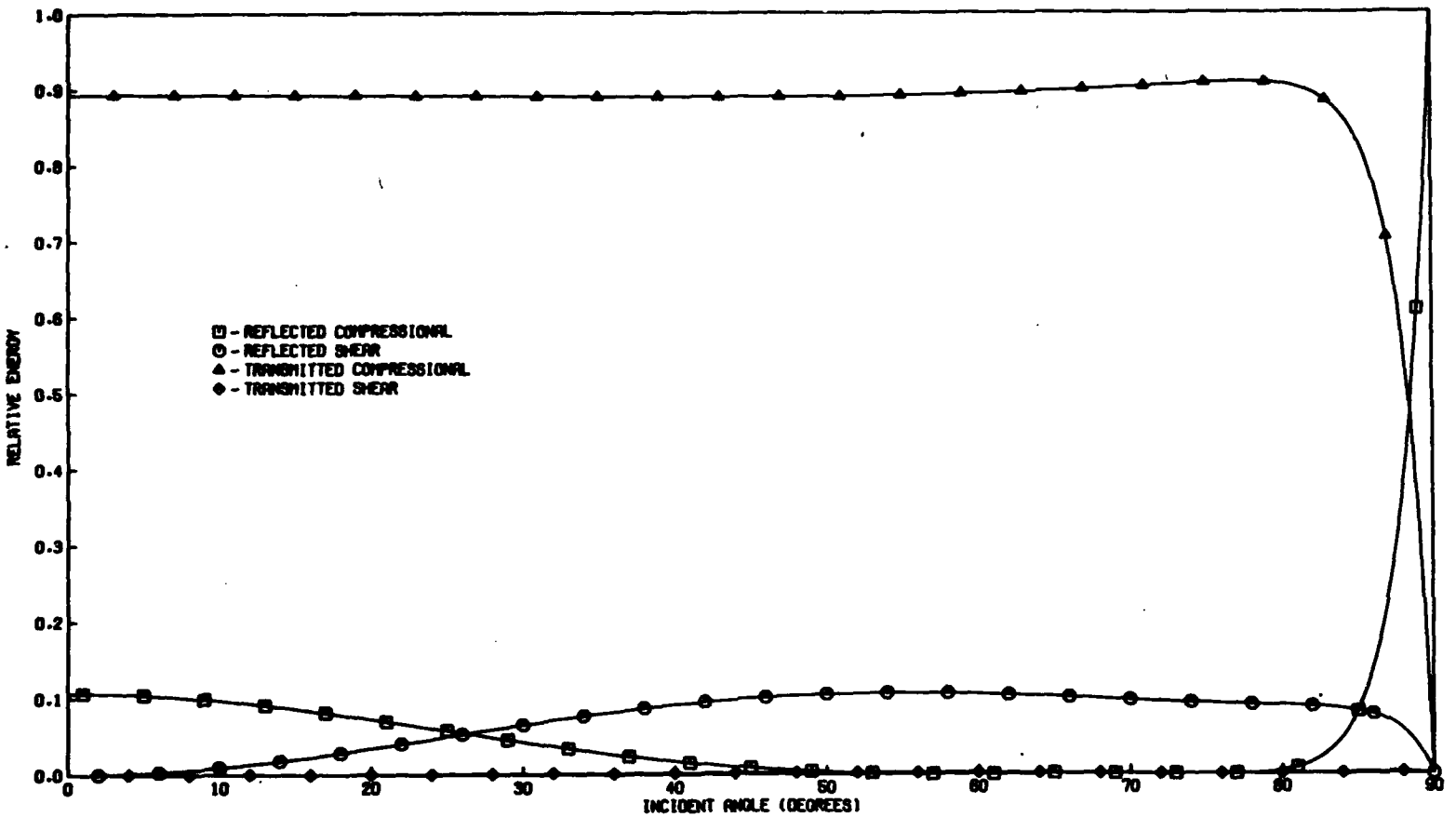


*Figure 22. Relative energy distribution of acoustic wave incident on permafrost-ice boundary, Hanover silt-ice (compressional wave incident).*

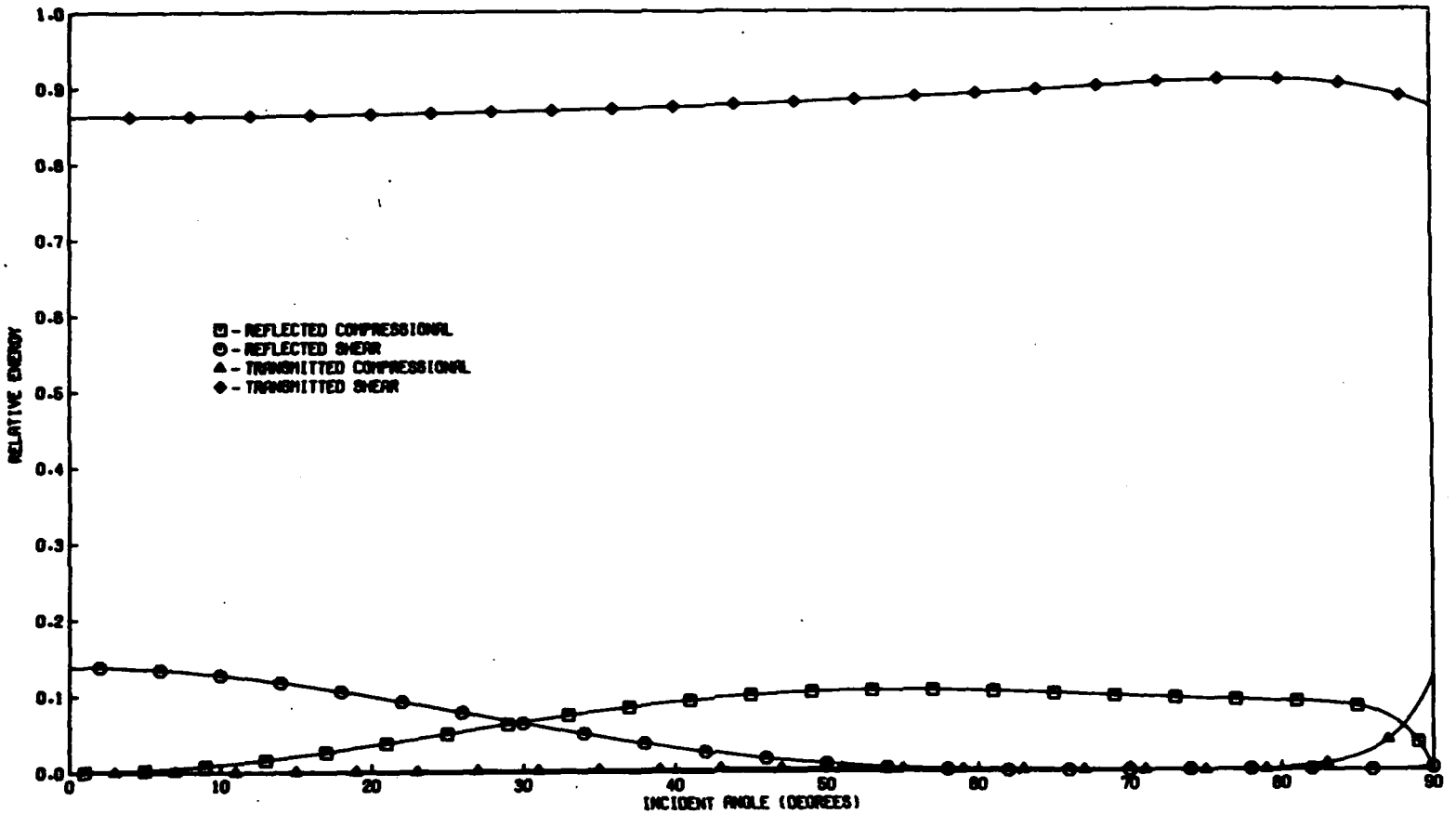


*Figure 23. Relative energy distribution of acoustic wave incident on permafrost-ice boundary. Hanover silt-ice (transverse wave incident).*

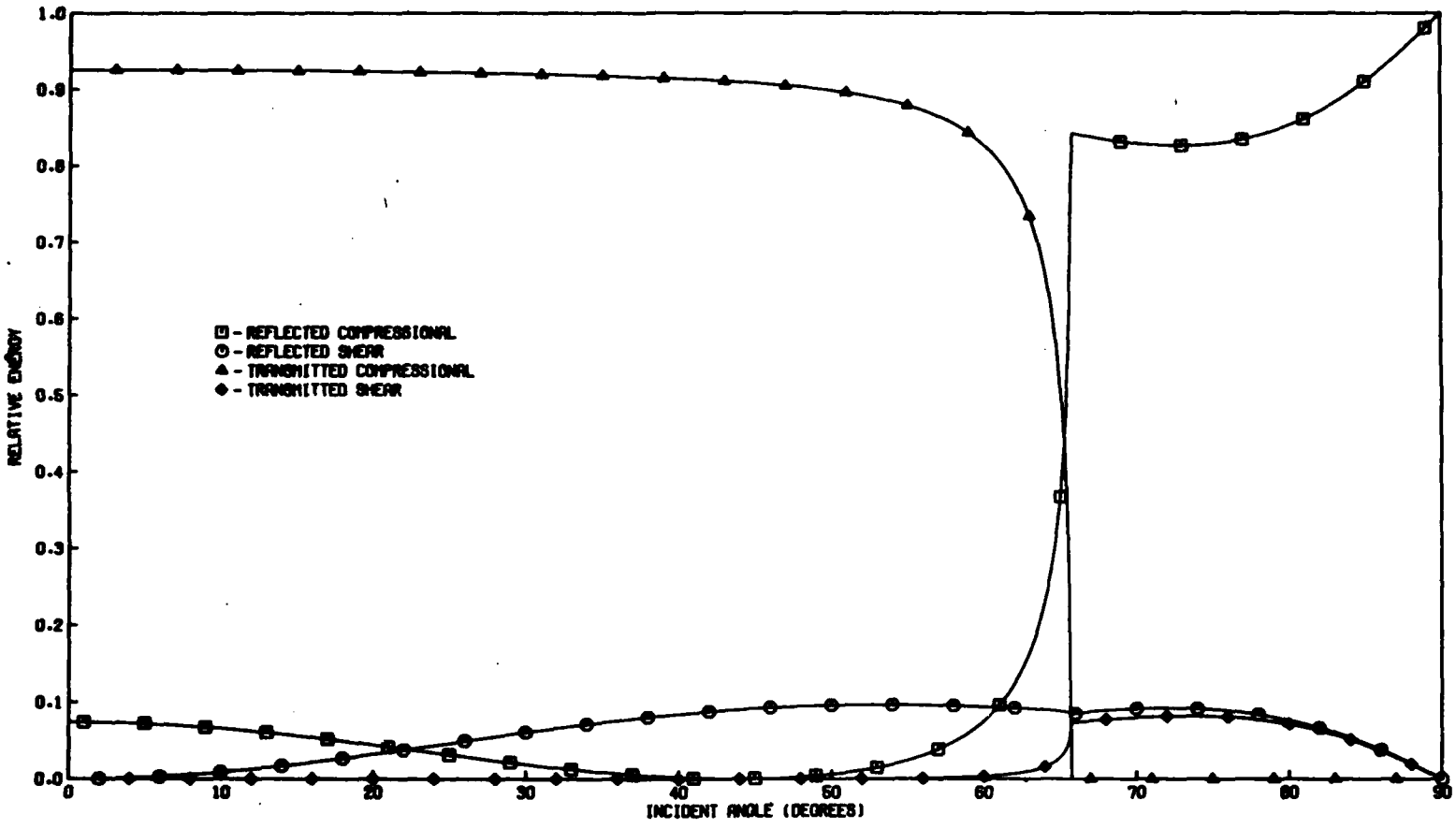


*Figure 24. Relative energy distribution of acoustic wave incident on permafrost-ice boundary, Goodrich clay-ice (compressional wave incident).*

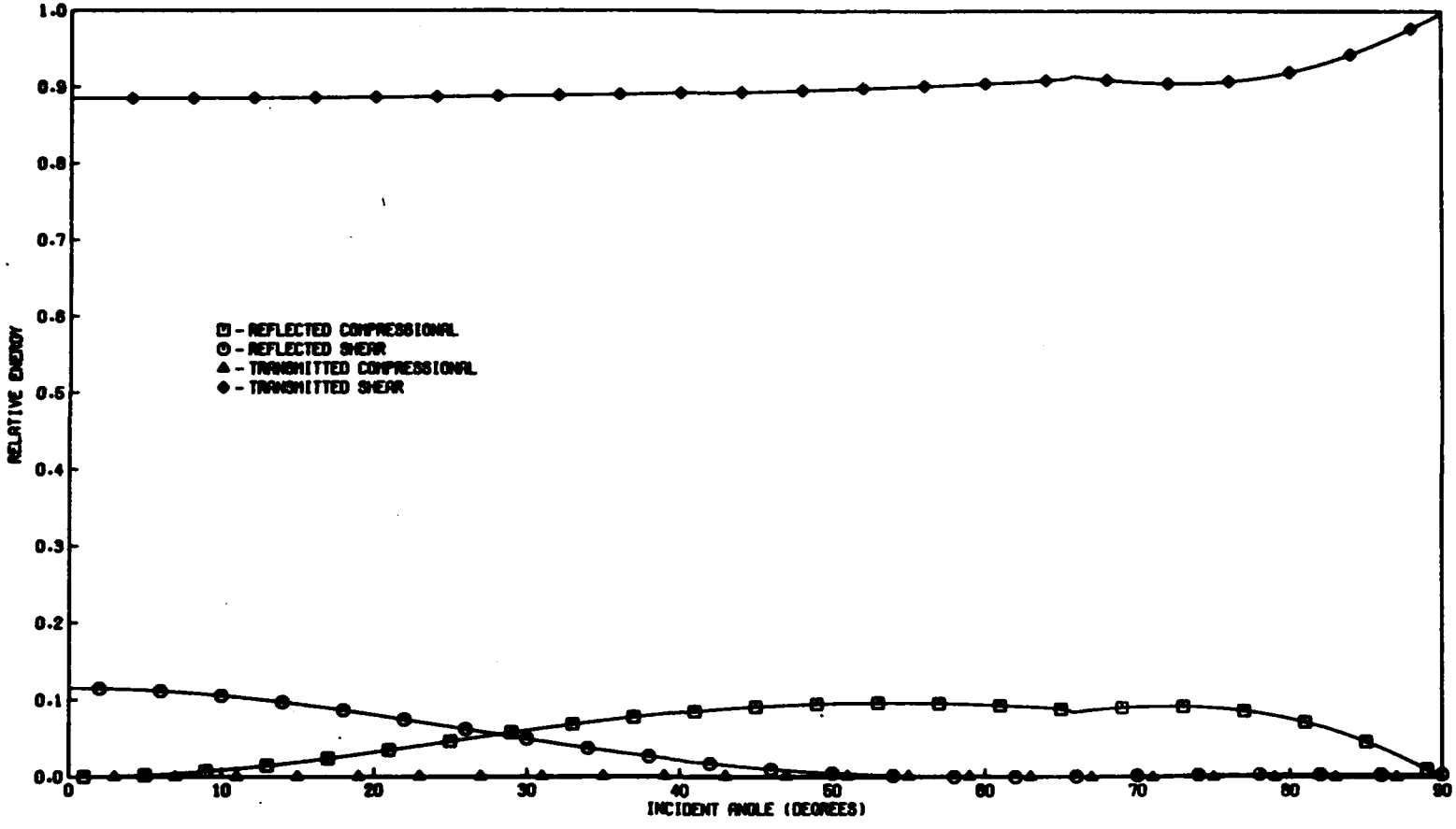


*Figure 25. Relative energy distribution of acoustic wave incident on permafrost-ice boundary, Goodrich clay-ice (transverse wave incident).*

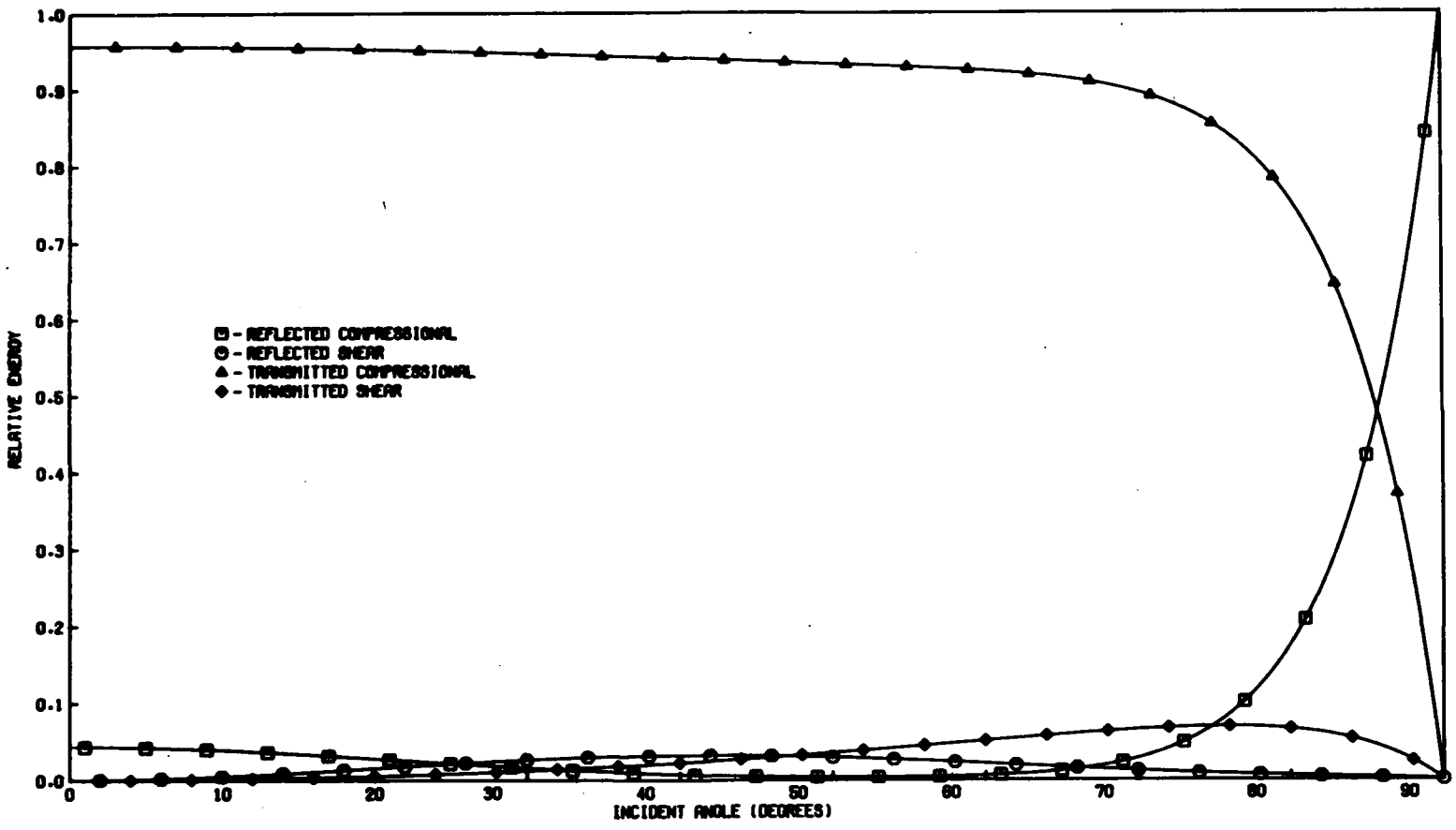


*Figure 26. Relative energy distribution of acoustic wave incident on boundary of two permafrost layers, Ottawa sand-Goodrich clay (compressional wave incident).*

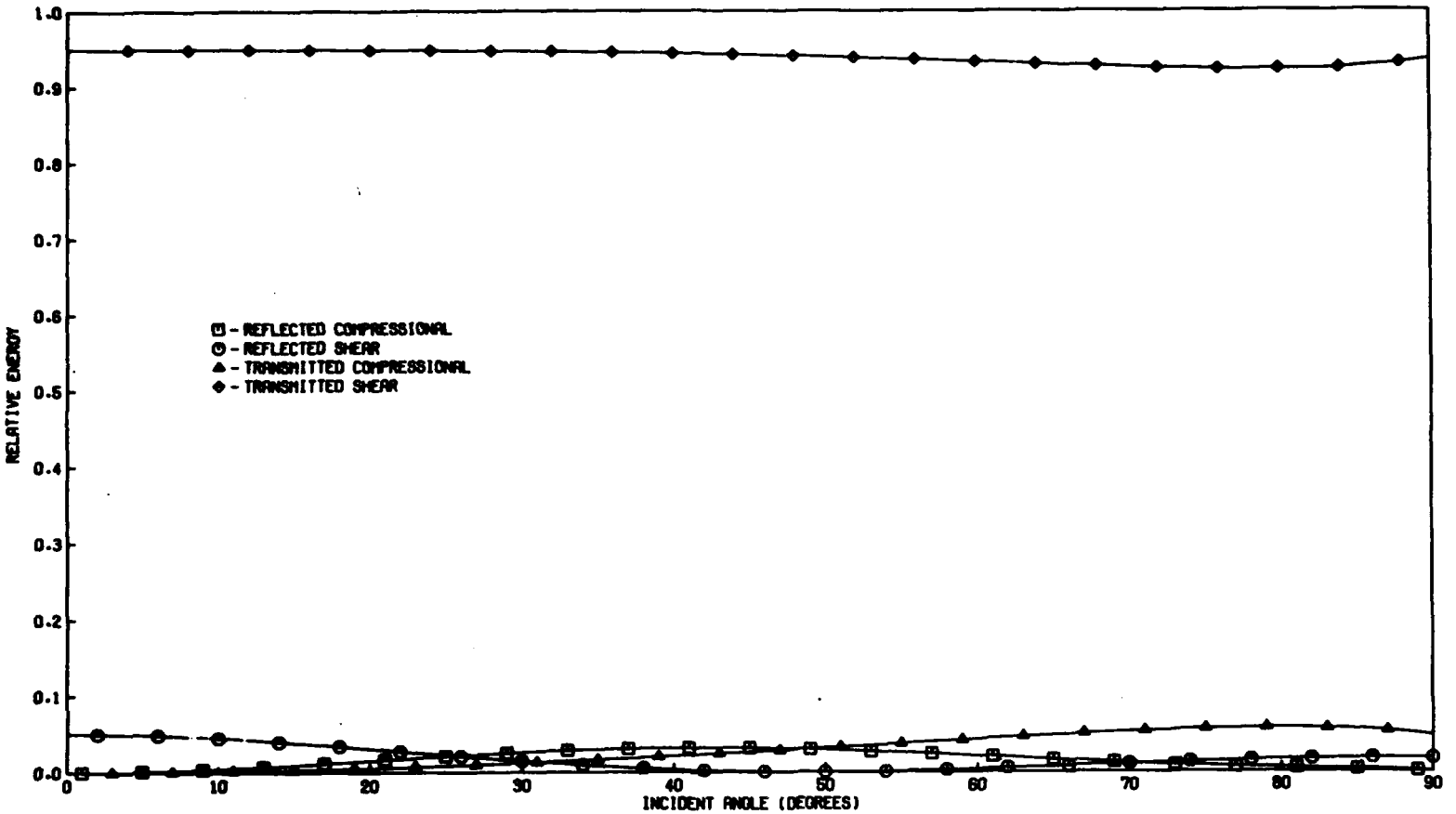


*Figure 27. Relative energy distribution of acoustic wave incident on boundary of two permafrost layers, Ottawa sand-Goodrich clay (transverse wave incident).*

To experimentally measure the reflectivity theoretically predicted above, the experiment diagrammed in Figure 28 was performed. In this test, an ice-permafrost boundary was formed as shown in Figure 29. A hydrophone was imbedded in the ice a known distance from both the surface and the interface. An acoustic transducer was coupled to the ice surface and pulsed. The amplitude of the acoustic wave was then recorded by the

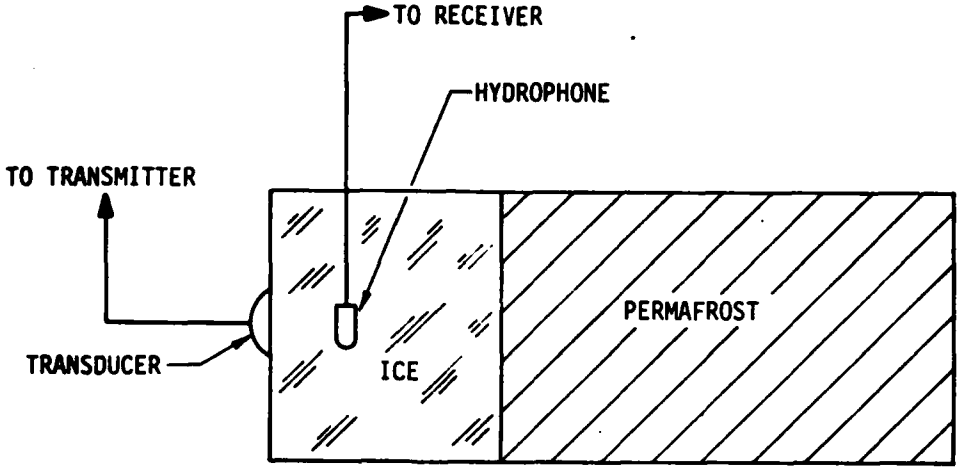


*Figure 28. Diagram of the reflectivity experiment.*

hydrophone both for the initial pulse and for the reflection from the interface. A typical result is shown in Figure 30. Correcting for attenuation losses in the ice, it was then possible to determine the energy loss at the boundary. The results of this measurement are shown in Table III. With the exception of Hanover silt, the losses observed during the test are clearly significantly larger than the theory predicted. There are many reasons for this result, including irregularities at the interface, inhomogeneous media, etc., but not the least of them is the existence of a transition layer. Figure 31 is a diagram of the transition layer problem.

*Table III. Results of reflectivity measurements (energy loss at the permafrost-ice boundary).*

| Material | Predicted Value | Measured Value |
|---|---|---|
| Ottawa Sand - Ice | 7.0 dB | 12.9 dB |
| Hanover Silt - Ice | 9.9 dB | 10.5 dB |
| Goodrich Clay - Ice | 8.3 dB | 16.2 dB |

*Figure 29. Photograph of test sample used in reflectivity measurement for ice-clay interface. (Note the condition of the clay surface.)*

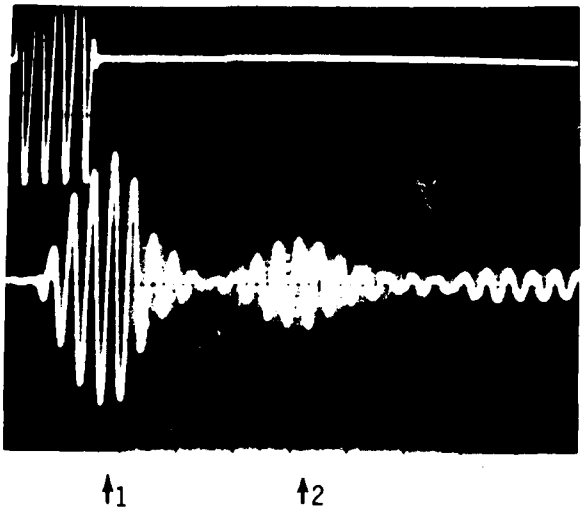


*Figure 30. Typical result of reflectivity measurement. (Arrow 1 denotes initial pulse; arrow 2 denotes reflected pulse.)*

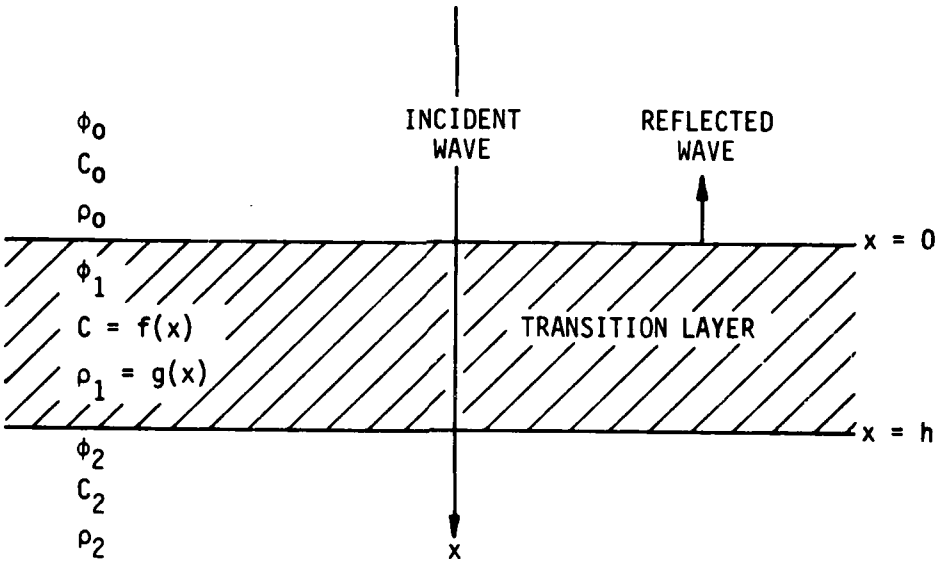


***Figure 31. Diagram of transition layer problem.***

The reflectivity of an acoustic plane wave normally incident on a layer between two isotropic media for which the velocity and density are dependent upon the depth into the layer is theoretically considered in Appendix A for the case of $C = (1+\alpha x)^n$ as a function of the thickness-to-wavelength ratio in the incident medium, $k_o h$. The results of this calculation for the special cases of n=1 (a linear transition between media) are shown in Figures 32-34. This calculation demonstrates that the effect of the layer is insignificant for wavelengths that are long compared to the thickness. However, when the wavelength becomes on the order of the thickness, the reflectivity becomes oscillatory with increasing $k_o h$. Thus, some knowledge of the interface between permafrost materials will be required to allow the experimenter to use acoustic frequencies that will result in the maximum energy possible being reflected from the boundary.

## CONCLUSIONS AND RECOMMENDATIONS

The feasibility of utilizing acoustic range-echo techniques to efficiently analyze subpermafrost structure to significant depths depends upon several factors. The more critical problems, those associated with the velocity and attenuation of the acoustic wave in the medium, with the acoustic impedance mismatch at boundaries between various constituents of permafrost, and with the modulation caused by possible transition layers, have been the subject of this study. The results of the research indicate that, if sufficient coupling between the sound source and the medium can be obtained, and if the acoustic wavelength is long compared to the majority of the scattering centers and to the transition layer between media, the utilization of pulse echo techniques could be a reasonable solution to the analysis problem.

Unfortunately, the results of the study are not as conclusive as one would like. It is therefore recommended that further basic research on the acoustic properties of permafrost materials be performed. Specifically, further test data should be obtained on the acoustic velocity and attenuation of permafrost samples for which the physical properties, i.e., saturation, homogeneity, etc., have been carefully controlled. Once the acoustic properties of these "idealized" permafrost samples are well understood, the tests should be expanded to include studying the acoustic properties of cores extracted from the environment, provided techniques exist to acquire these samples without disturbing their physical composition. If not, in situ measurements should be performed prior to the extraction of the permafrost cores.

Finally, it is of great importance to initiate a program to study the physical properties of transition layers between various constituents of permafrost. Although the experimenter can optimize his tests for depth and resolution by adjusting the acoustic frequency, unless the transition zones can be successfully modeled, successful and efficient subsurface permafrost reflectivity measurements will never be achieved.

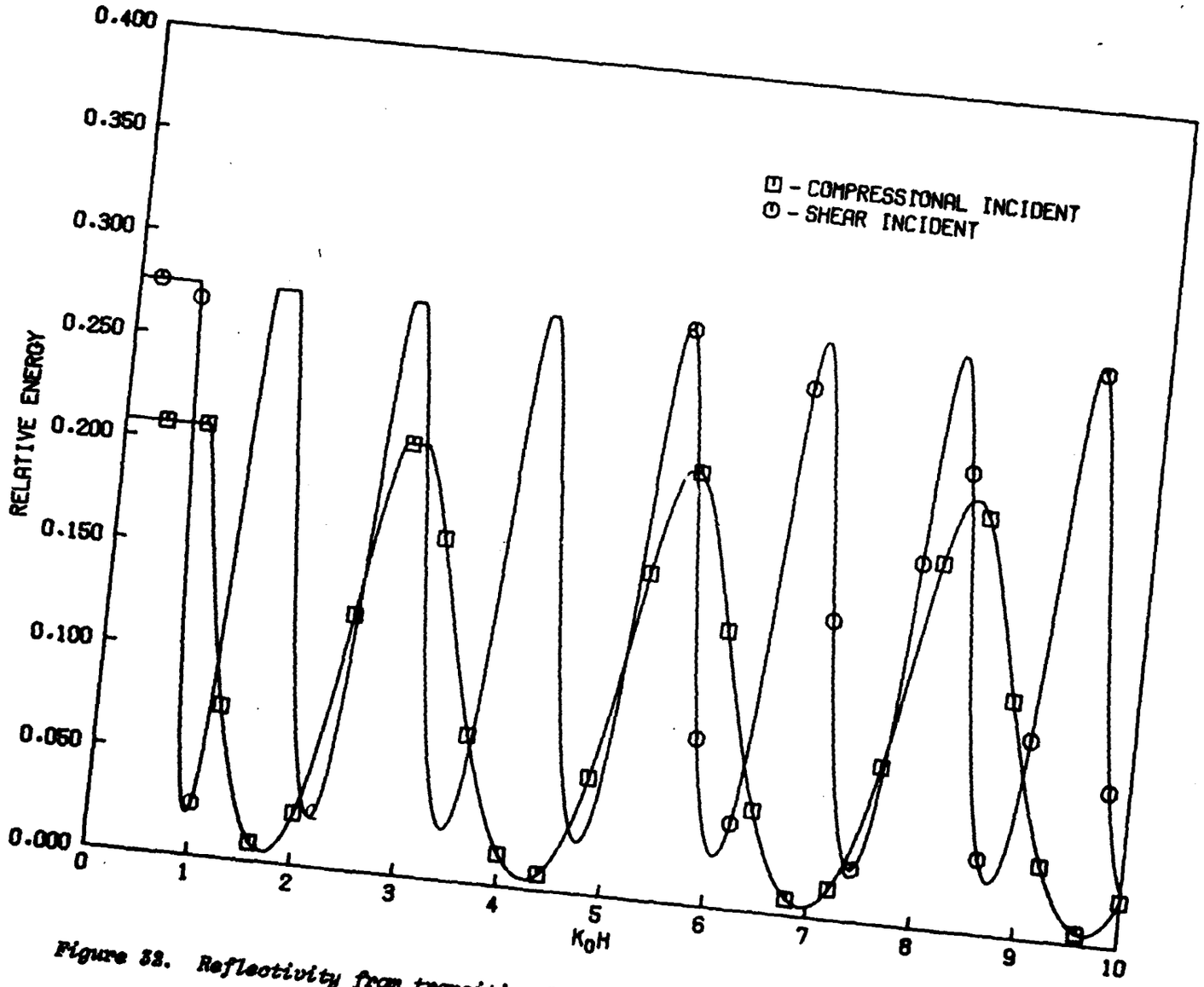


*Figure 33. Reflectivity from transition layer; Ottawa sand-ice; velocity = $(1+AX)^2$*

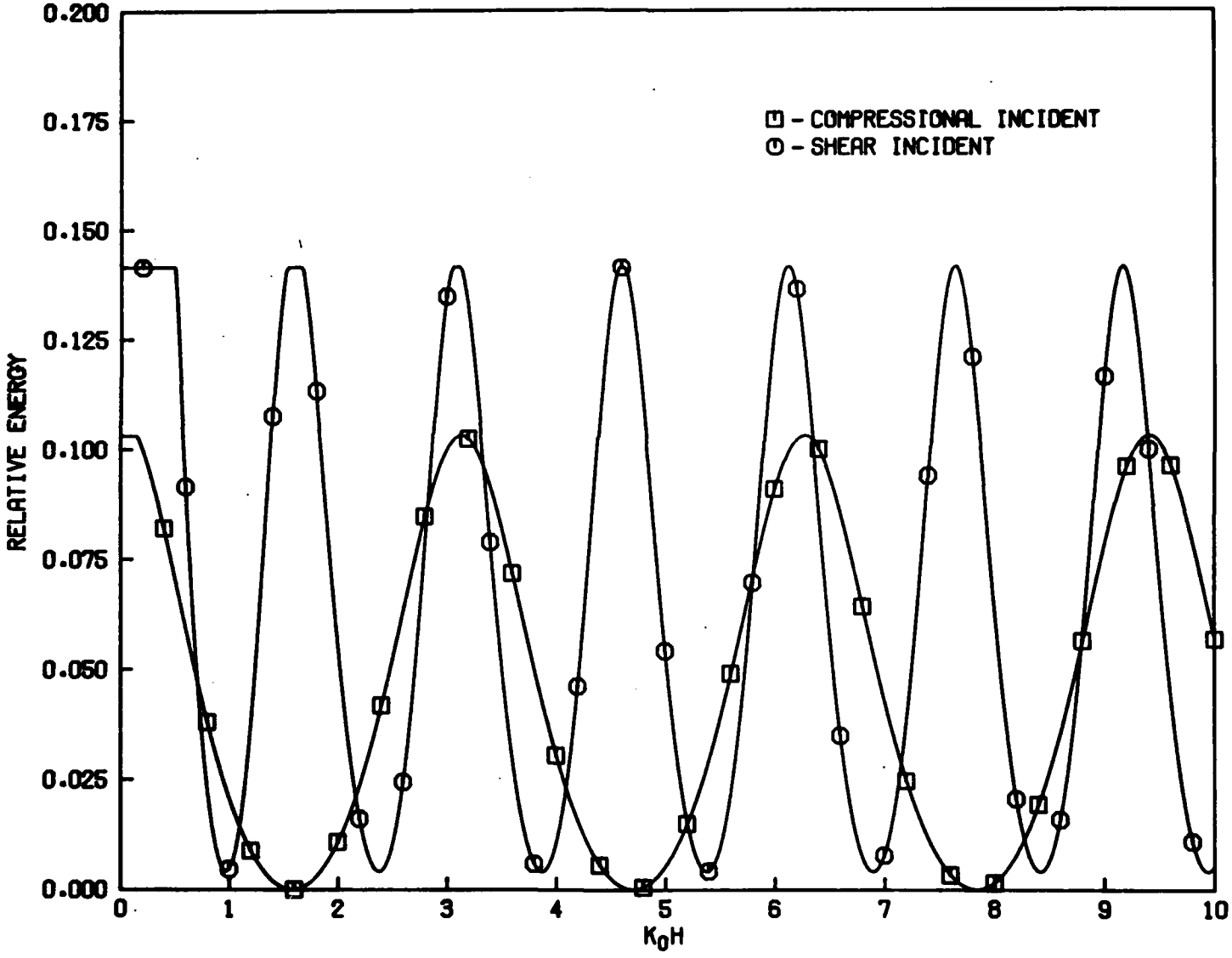


*Figure 33. Reflectivity from transition layer; Hanover silt-ice; velocity = $(1+AX)^1$*

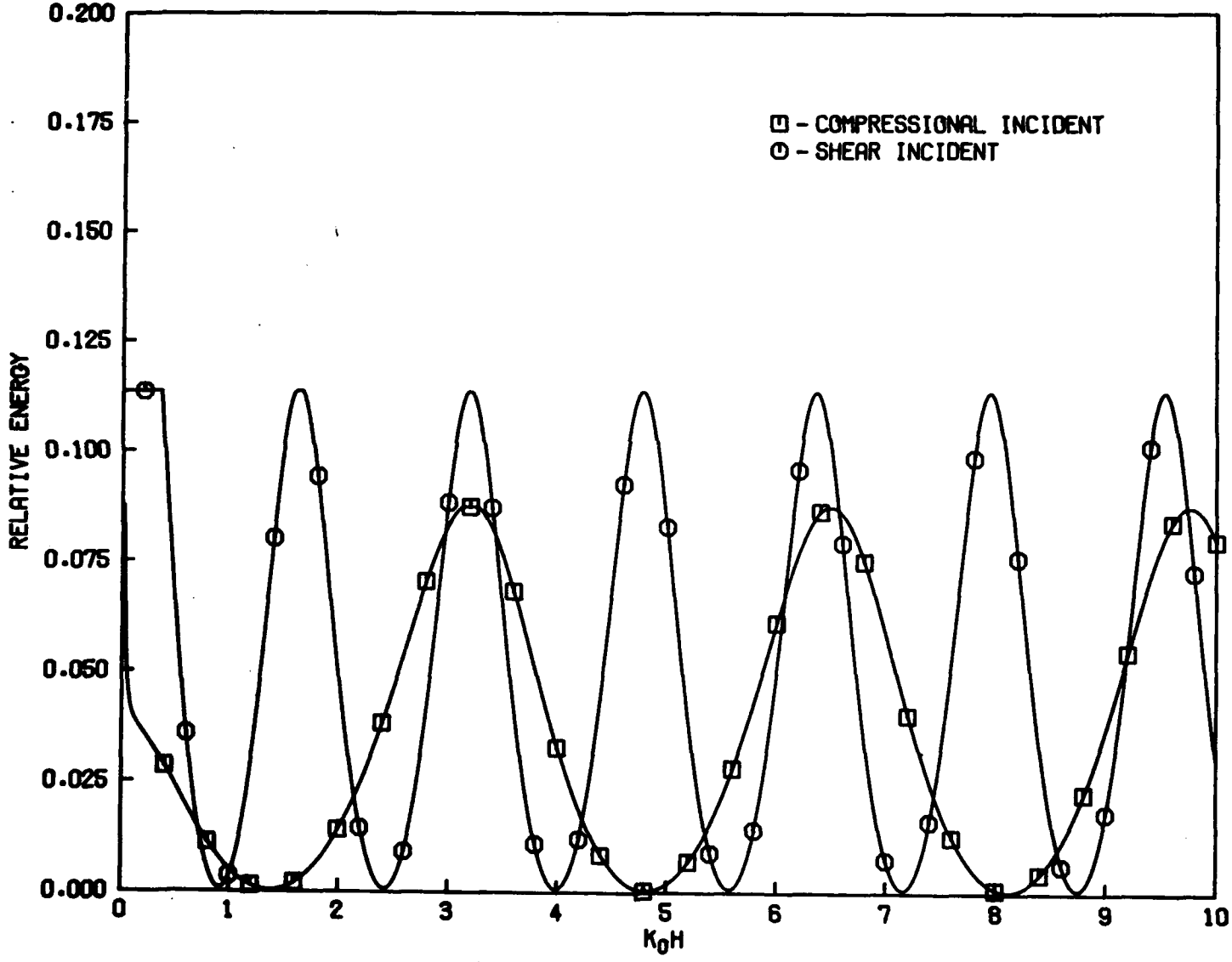


*Figure 34. Reflectivity from transition layer; Goodrich clay - ice; velocity = $(1+AX)^1$*

# APPENDIX A

## THEORIES

# I. THEORY OF ACOUSTIC REFLECTION AND TRANSMISSION AT AN INTERFACE

## A. Ideal Case

Consider an acoustic plane wave striking an interface between two elastic media as shown in Figure A1. It is assumed that each medium is isotropic and homogeneous. Complexities, such as viscoelastic properties, are not considered. Each medium is characterized by its density, Lame' constant and shear modulus. Finally, it is assumed that strong coupling exists at the interface.

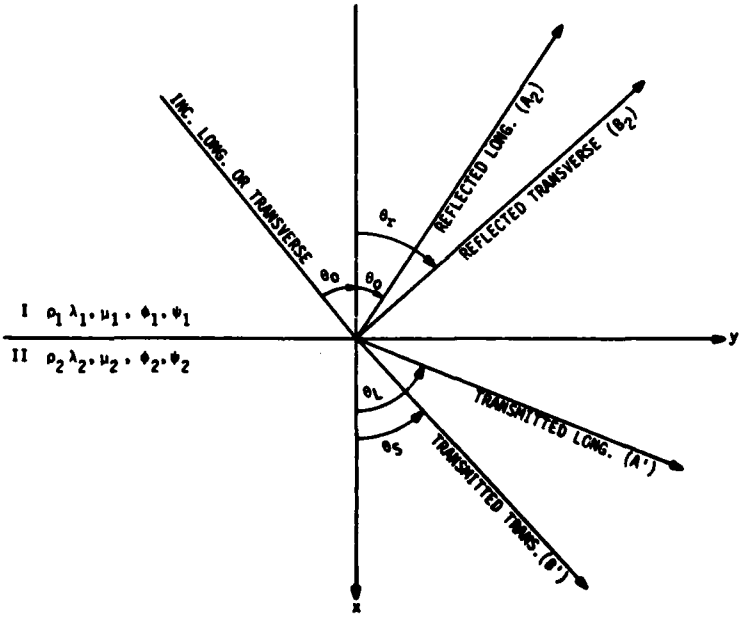


*Figure A1. Acoustic wave reflection and transmission at an interface.*

The displacement potential functions are then given by

$$\phi_1 = e^{i(\omega t-\beta y)} \left[\delta_L e^{-i\alpha_o x} + A_2 e^{i\alpha_o x}\right]$$

$$\psi_1 = e^{i(\omega t-\beta y)} \left[(1-\delta_L)\ e^{-i\alpha_S x} + B_2 e^{i\alpha_S x}\right] \qquad \text{(A1)}$$

$$\phi_2 = e^{i(\omega t-\beta y)}\ A' e^{-i\alpha_L x}$$

$$\psi_2 = e^{i(\omega t-\beta y)}\ B' e^{-i\alpha_T x} ,$$

where

$$\delta_L = \begin{cases} 1 & \text{incident compressional wave} \\ 0 & \text{incident transverse wave} \end{cases}$$

and

$$\beta = k_o \sin\theta_o = k_S \sin\theta_S = k_L \sin\theta_L = k_T \sin\theta_T$$

$$\alpha_o = k_o \cos\theta_o$$

$$\alpha_S = k_S \cos\theta_S$$

$$\alpha_L = k_L \cos\theta_L$$

$$\alpha_T = k_T \cos\theta_T$$

$$\theta_S = \sin^{-1}\left(\frac{k_o}{k_S}\sin\theta_o\right)$$

$$\theta_L = \sin^{-1}\left(\frac{k_o}{k_L}\sin\theta_o\right)$$

$$\theta_T = \sin^{-1}\left(\frac{k_o}{k_T}\sin\theta_T\right) .$$

At the boundary x=0, the normal displacement, pressure and shear stress are continuous. Also, since strong coupling has been assumed, the tangen-

tial displacement is also continuous. Mathematically, this is expressed as

$$
\begin{aligned}
u_x^I &= u_x^{II} \\
u_y^I &= u_y^{II} \\
\sigma_{xx}^I &= \sigma_{xx}^{II} \\
\sigma_{xy}^I &= \sigma_{xy}^{II} \quad ,
\end{aligned}
\tag{A2}
$$

where

$$
\begin{aligned}
\vec{u} &= \text{grad } \phi + \text{curl } \vec{\psi} \\
\vec{\psi} &= (0,0,\psi) \\
\sigma_{ij} &= \lambda \delta_{ij} \nabla^2 \phi + 2\mu S_{ij} \\
S_{ij} &= \frac{1}{2}\left(\frac{\partial u_i}{\partial x_j} + \frac{\partial u_j}{\partial x_i}\right) \\
\delta_{ij} &= \begin{cases} 1 & i=j \\ 0 & i \neq j \end{cases} \quad ,
\end{aligned}
\tag{A3}
$$

and i and j denote direction. Applying the boundary conditions then gives four simultaneous equations

$$A_2 - \frac{\beta}{\alpha_o} B_2 + \frac{\alpha_L}{\alpha_o} A' + \frac{\beta}{\alpha_o} B' = \delta_L + \frac{\beta}{\alpha_o}(1-\delta_L)$$

$$A_2 + \frac{\alpha_S}{\beta} B_2 - A' + \frac{\alpha_T}{\beta} B' = -\delta_L + \frac{\alpha_T}{\beta}(1-\delta_L)$$

$$-\left(1 - \frac{2\beta^2}{k_S^2}\right) A_2 + \frac{2\beta\alpha_S}{k_S^2} B_2 + \frac{\rho_2}{\rho_1}\left(1 - \frac{2\beta^2}{k_T^2}\right) A' + \frac{\rho_2}{\rho_1}\frac{2\beta\alpha_T}{k_T^2} B' = \left(1 - \frac{2\beta^2}{k_S^2}\right)\delta_L + \frac{2\beta\alpha_S}{k_S^2}(1-\delta_L) \qquad \text{(A4)}$$

$$\frac{2\alpha_o\beta}{k_S^2} A_2 + \left(1 - \frac{2\beta^2}{k_S^2}\right) B_2 + \frac{\rho_2}{\rho_1}\frac{2\beta\alpha_L}{k_T^2} A' - \frac{\rho_2}{\rho_1}\left(1 - \frac{2\beta^2}{k_T^2}\right) B' = \frac{2\alpha_o\beta}{k_S^2}\delta_L - \left(1 - \frac{2\beta^2}{k_S^2}\right)(1-\delta_L) ,$$

which have been solved using program SOLID in Appendix B to calculate the energies of reflection and transmission at the interface for several examples. The results of the calculation are shown in Figures 20-27 of the text.

## B. Extension of the Theory to Include a Transition Layer

The problem to be solved is diagrammed in Figure A2. An incident plane compressional* wave is incident on the boundary of a layer in which the velocity and/or the density is a function of depth into the medium. The displacement potentials are given by

$$\phi_o = (e^{-ik_o x} + A_2 e^{ik_o x}) e^{i\omega t}$$

$$\phi_1 = (B_1 e^{-ik_L x} + B_2 e^{ik_L x}) e^{i\omega t} \qquad \text{(A5)}$$

$$\phi_2 = C e^{ik_C x} e^{i\omega t} ,$$

*Development of the theory for an incident transverse wave is equivalent to the development presented here.

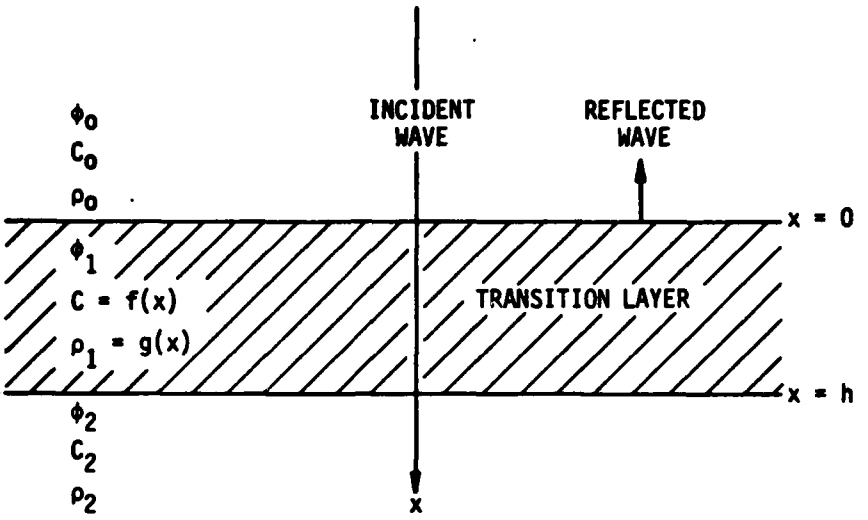


*Figure A2. Diagram of transition layer problem.*

where now $k_L$ is a function of x. At the boundaries x=0 and x=h the normal displacement and pressure are continuous,* where the displacements and stresses are defined by Eq. (A3). Evaluating the boundary conditions yields four simultaneous equations to be solved for the amplitudes:

$$k_o(1-A_2) = k_L\Big|_{x=o}(B_1-B_2)$$

$$\rho_o(1-A_2) = \rho_1\left[(B_1+B_2) + \frac{2i}{k_L^2}\frac{\partial k_L}{\partial x}\Big|_{x=o}(B_1-B_2)\right]$$

$$\left(k_L+h\frac{\partial k_L}{\partial x}\right)\left(B_1 e^{-ik_Lh} - B_2 e^{ik_Lh}\right)\Big|_{x=h} = k_C c\, e^{-ik_Ch} \qquad \text{(A6)}$$

*For the case of a shear wave incident, the tangential displacement and shear stress are continuous where it has been assumed that strong coupling exists at the boundaries.

$$\frac{\rho_1}{k_L^2}\left\{\left[\left(k_L+h\frac{\partial k_L}{\partial x}\right)^2+i\left(2\frac{\partial k_L}{\partial x}+h\frac{\partial^2 k_L}{\partial x^2}\right)\right]B_1 e^{-ik_Lh}+\left[\left(k_L+h\frac{\partial^2 k_L}{\partial x^2}\right)^2\right.\right.$$

$$\left.\left.-i\left(2\frac{\partial k_L}{\partial x}+h\frac{\partial k_L}{\partial x^2}\right)\right]B_2 e^{ik_Lh}\right\}\Big|_{x=h}=\rho_2 Ce^{-ik_Ch} \quad ,$$

which are completely general.

Consider the special case for which the functional dependence of the velocity in the transition region is given by

$$C_L = C_o(1+\alpha x)^n \quad , \tag{A7}$$

where $\alpha$ is the gradient and n is the order of dependence and need not necessarily be an integer. It can then be shown that the amplitude of the reflected wave is given by

$$A_2 = \frac{\left[\frac{\rho_1}{\rho_o}\frac{(\gamma+1)}{(\gamma-1)}-1\right]-\frac{2in\alpha}{k_o}}{\left[\frac{\rho_1}{\rho_o}\frac{(\gamma+1)}{(\gamma-1)}+1\right]-\frac{2in\alpha}{k_o}} \quad , \tag{A8}$$

where

$$\frac{\rho_1}{\rho_o}\frac{(\gamma+1)}{(\gamma-1)}-1=\frac{\left[\frac{\rho_2}{\rho_o}\frac{k_o}{k_C}p+q\right]+r\tan k_Lh+i\left\{r+\left[q-\frac{k_o}{k_C}p\right]\tan k_Lh\right\}}{q-r\tan k_Lh+i\frac{k_o}{k_C}p\tan k_Lh}$$

$$\frac{\rho_1}{\rho_o}\frac{(\gamma+1)}{(\gamma-1)}+1=\frac{\left[\frac{\rho_2}{\rho_o}\frac{k_o}{k_C}p+q\right]-r\tan k_Lh+i\left\{r+\left[q+\frac{k_o}{k_C}p\right]\tan k_Lh\right\}}{q-r\tan k_Lh+i\frac{k_o}{k_C}p\tan k_Lh}$$

$$p = \frac{[1 - (n-1)\alpha h]}{(1+\alpha h)^{n-1}}$$

$$q = [1 - (n-1)\alpha h]^2$$

$$r = \frac{2\alpha n}{k_o} (1+\alpha h)^n \left[1 - \frac{1}{2} (n-1)\alpha h\right] .$$

These equations have been evaluated using the computer program TRNTION given in Appendix B for the special cases of n=1 and n=2. The results of this calculation are shown in Figures 32-34 of the text.

## II. APPROXIMATION OF ATTENUATION

The attenuation of a sound wave propagating in a material that is not perfectly elastic, homogeneous and isotropic can be considered to be the result of two mechanisms: (1) dissipation processes originating from internal friction, anelastic behavior of the material, thermal dissipation, viscous slippage at crystal boundaries, etc., and (2) scattering originating from the interaction of the acoustic wave with scattering centers in the medium. The relative contribution of each of these mechanisms to the total attenuation depends on the frequency of the sound wave. At low frequencies, the wavelength of the sound is very large compared to the scattering centers; therefore, the scattering cross section, i.e., the relative amount of energy scattered out of the incident wave, is extremely small and the attenuation is due almost entirely to dissipation. As the frequency increases, the attenuation due to scattering becomes more important until, when the wavelength becomes approximately on the order of the size of the scattering center, scattering predominates. Thus, to assess the frequency dependence of the attenuation, the dissipation and scattering processes must both be evaluated.

## A. Long Wavelength Isotropic Solutions

For wavelengths that are long compared to the size of the scattering center the calculation of acoustic velocity and attenuation can be derived ignoring the contributions due to scattering. Even though not all of the internal mechanisms contributing to the dissipation processes are known, the general theory can be developed by grouping all attenuation into a common source. This is accomplished mathematically[26] by the replacement of the shear modulus (M) and the Lame´ constant ($\Lambda$) in the elastic stress-strain relationship by the first order differential operators

$$M = \mu + \mu' \frac{\partial}{\partial t}$$
$$\Lambda = \lambda + \lambda' \frac{\partial}{\partial t} \quad . \tag{A9}$$

In Eq. (1), the unprimed terms denote the elastic and the primed terms denote the viscous (or attenuative) contributions.

Consider an acoustic shear wave* moving in the positive (downward) x-direction. The displacement potential is given by

$$\psi = Ae^{i(\omega t - \alpha x)} \quad , \tag{A10}$$

where

$\omega$ is the circular frequency

$t$ is the time

$\alpha$ is the complex wavenumber.

*The derivation for the compressional wave propagation is similar to that presented here, the difference being the introduction of the $(\Lambda + 2M)$ operator in the wave equation, Eq. (A11), rather than the shear modulus (M) operator. The displacement potential must, of course, be associated with the compressional rather than the transverse wave.

This displacement potential obeys the wave equation

$$\rho \frac{\partial^2 \psi}{\partial t^2} = M \nabla^2 \psi \ , \tag{A11}$$

where $\rho$ is the density of the medium and $\nabla^2$ is the Laplacian operator. Substitution of Eqs. (A9) and (A10) into Eq. (A11) and carrying out the operations gives the relation

$$\rho\omega^2 = \alpha^2 \ (\mu + i\omega\mu') \ . \tag{A12}$$

For an attenuative medium, the complex wavenumber can be written as

$$\alpha = k - i\tau \ , \tag{A13}$$

where

$k$ is the running vector, $\omega/c$

$c$ is the wave velocity

$\tau$ is the generalized attenuation.

Making this substitution into Eq. (A12) and separating the real and imaginary components yields the simultaneous equations

$$\begin{aligned} \rho\omega^2 &= \mu(k^2 - \tau^2) + 2\mu'\omega k\tau \\ 0 &= \omega\mu'(k^2 - \tau^2) - 2\mu k\tau \ . \end{aligned} \tag{A14}$$

Setting

$$R = \frac{\mu'}{\mu} \ ,$$

these equations have the solutions

$$\tau = \frac{k}{R\omega}\left\{\sqrt{1 + R^2\omega^2} \quad -1\right\}$$

$$k^2 = \frac{1}{2}\frac{\rho\omega^2}{\mu}\left\{\frac{\sqrt{1 + R^2\omega^2} \quad + 1}{1 + R^2\omega^2}\right\} \quad , \tag{A15}$$

where now both $\mu$ and R may be frequency dependent. The procedure from this point is to introduce a mathematical model of the medium composed of elastic and viscous constants that are frequency independent, and then fit the results to experimental data.

Maxwell[27] suggested that viscoelastic materials could be represented by an elastic element (spring) in series with a viscous element (dashpot) as shown in Figure A3. Voigt[28] placed these elements in parallel as in Figure A4. Detailed mathematical analyses of these as well as more complex models are covered in standard texts[29-31] and will not be discussed here. However, it can be shown that for the Maxwell model

$$\tau = \frac{k\eta_m\omega}{E_m}\left\{\sqrt{1 + \left(\frac{E_m}{\eta_m\omega}\right)^2} - 1\right\}$$

$$k^2 = \frac{\rho\omega^2}{2\mu}\left\{\frac{\sqrt{1 + \left(\frac{E_m}{\eta_m\omega}\right)^2} + 1}{1 + \left(\frac{E_m}{\eta_m\omega}\right)^2}\right\} \quad ,$$

where

$$\mu = \frac{E_m\omega^2}{\left(\frac{E_m}{\eta_m}\right)^2 + \omega^2}$$

and

$$R\omega = \frac{E_m}{\eta_m \omega} .$$

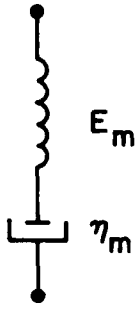


*Figure A3. Maxwell's mechanical representation of viscoelastic solids.*

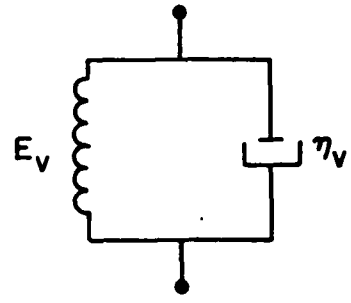


*Figure A4. Voigt's mechanical representation of viscoelastic solids.*

For the Voigt model

$$\tau = \frac{kE_v}{\eta_v \omega}\left\{\sqrt{1 + \left(\frac{\eta_v}{E_v}\omega\right)^2} - 1\right\}$$

$$k^2 = \frac{1}{2}\frac{\rho\omega^2}{E_v}\left\{\frac{\sqrt{1 + \left(\frac{\eta_v}{E_v}\omega\right)^2} + 1}{1 + \left(\frac{\eta_v}{E_v}\omega\right)^2}\right\} .$$

where

$$\mu = E_v$$

$$R\omega = (E_v/\eta_v)\omega .$$

Very few solids behave like either the Maxwell or the Voigt model. However, since more complicated models become extremely involved mathematically, and because models specifying a greater number of parameters require more experimental evidence to substantiate their validity, using a single Maxwell or Voigt element is a convenient method of obtaining a first order approximation of a viscoelastic solid's mechanical properties.

## B. Short Wavelength Solution

To estimate the contribution due to scattering, consider the problem shown in Figure A5. An acoustic plane wave propagating in an isotropic elastic solid encounters a spherical scatterer which, for this discussion, is also assumed to be elastic. Both media are characterized by their

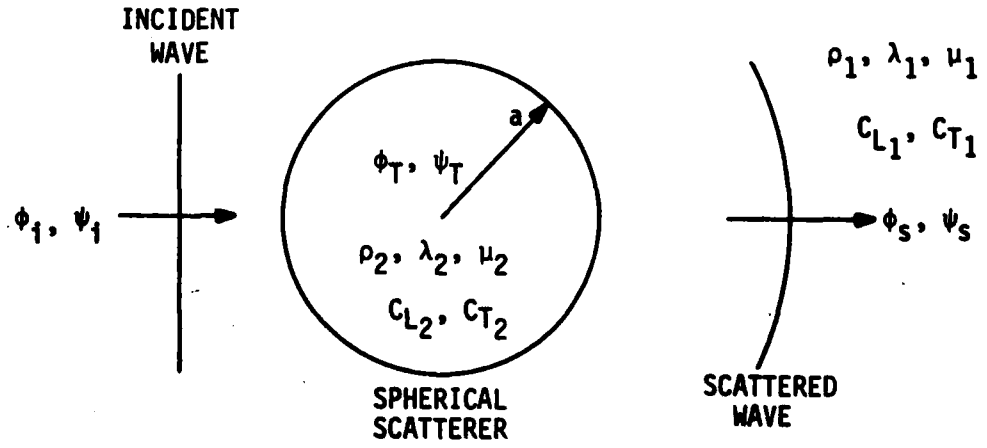


*Figure A5. Representation of the problem.*

densities ($\rho_i$), shear moduli ($\mu_i$) and Lame´ constants ($\lambda_i$). Elasticity theory defines the velocities as

$$C_{L_i} = \sqrt{\frac{\lambda_i + 2\mu_i}{\rho_i}} = \frac{\omega}{k_i}$$
$$C_{T_i} = \sqrt{\frac{\mu_i}{\rho_i}} = \frac{\omega}{K_i} \quad , \tag{A18}$$

where $\omega$ is the circular frequency and $k_i$ and $K_i$ are the wavenumbers of the compressional and transverse wave, respectively. The displacement can be written in terms of the displacement potentials $\phi$ and $\psi$ as

$$\vec{u} = \text{grad}\ \phi + \text{curl}\ \vec{\psi} \ . \tag{A19}$$

For spherical coordinates,

$$\vec{u} = -\nabla\phi + \nabla x \nabla x (\vec{r}\psi) \ . \tag{A20}$$

The displacement potentials are of the form

$$\sum_{m=0}^{\infty} C_m f_m(pr)\ P_m(\cos\theta)\ e^{i\omega t} \quad , \tag{A21}$$

where

$f_m(pr)$ = the spherical Bessel function of order m

p = either k or K, depending upon the wave considered

$P_m(\cos\theta)$ = the Legendre polynomial of order m.

When the incident plane wave strikes the scattering center, some of the energy is scattered away and some is transmitted through the scatterer. Since all the waves must obey the same wave equations, the wave potentials, neglecting the time dependence, may be written as

$$\phi \text{ Incident} = \sum_{m=0}^{\infty} I_{cm}\, j_m (k_1 r)\, P_m (\cos\theta)$$

$$\psi \text{ Incident} = \sum_{m=0}^{\infty} I_{sm}\, j_m (K_1 r)\, P_m (\cos\theta) \qquad \text{(A22)}$$

$$\phi \text{ Scattered} = \sum_{m=0}^{\infty} A_m\, h_m (k_1 r)\, P_m (\cos\theta)$$

$$\psi \text{ Scattered} = \sum_{m=0}^{\infty} B_m\, h_m (K_1 r)\, P_m (\cos\theta)\ , \qquad \text{(A23)}$$

$$\phi \text{ Transmitted} = \sum_{m=0}^{\infty} C_m\, j_m (k_2 r)\, P_m (\cos\theta)$$

$$\psi \text{ Transmitted} = \sum_{m=0}^{\infty} D_m\, j_m (K_2 r)\, P_m (\cos\theta) \qquad \text{(A24)}$$

where r and θ are spherical coordinates. The spherical Bessel functions of the first kind, $j_m(kr)$, and third kind, $h_m(kr)$, are used to assure that the scattered wave is propagating away from the scatterer located at the origin of the coordinate system. In order for the incident wave to be plane and of unit amplitude, $I_{cm}$ and $I_{sm}$ must be of the form[32]

$$I_m = \frac{(-i)^{m+1}}{P} (2m+1)\ , \qquad \text{(A25)}$$

where p is k and K, respectively. The coefficients $A_m$, $B_m$, $C_m$, and $D_m$ are determined by the boundary conditions at the scattering surface. For a solid-solid interface assuming strong coupling, these boundary conditions are

(a) Radial displacement continuous

(b) Tangential displacement continuous

(c) Radial stress continuous

(d) Tangential stress vanishes.

At the boundary, r = a, these conditions can be written mathematically as

$$\begin{aligned}
&\text{(a)}\quad u_{r(inc)} + u_{r(scatt)} = u_{r(trans)} \\
&\text{(b)}\quad u_{\theta(inc)} + u_{\theta(scatt)} = u_{\theta(trans)} \\
&\text{(c)}\quad \sigma_{rr(inc)} + \sigma_{rr(scatt)} = \sigma_{rr(trans)} \\
&\text{(d)}\quad \sigma_{r\theta(inc)} + \sigma_{r\theta(scatt)} = \sigma_{r\theta(trans)} \, .
\end{aligned} \tag{A26}$$

In terms of the displacement potentials, the stress and displacement components of Eq. (A25) are

$$\begin{aligned}
\sigma_{rr} &= \rho\omega^2 \left\{ \phi + \frac{2}{K^2} \left[ \frac{2}{r} \frac{\partial \phi}{\partial r} + \frac{1}{r^2} \Omega\phi - \frac{\partial}{\partial r} \left( \frac{1}{r} \Omega \psi \right) \right] \right\} \\
\sigma_{\theta r} &= -2 \frac{\rho\omega^2}{K^2} \frac{\partial}{\partial \theta} \left[ \frac{1}{r} \frac{\partial \phi}{\partial r} - \frac{1}{r^2} \phi + \frac{1}{r} \frac{\partial \psi}{\partial r} + \frac{1}{r^2} \left( 1 + \frac{K^2 r^2}{2} \right) \psi + \frac{1}{r^2} \Omega \psi \right] , \\
u_r &= - \left[ \frac{\partial \phi}{\partial r} + \frac{1}{r} \Omega \psi \right]
\end{aligned} \tag{A27}$$

where

$$\Omega = \frac{1}{\sin\theta} \frac{\partial}{\partial \theta} \left( \sin\theta \frac{\partial}{\partial \theta} \right) \, . \tag{A28}$$

The scattering cross section is determined by calculating the ratio of the time rate at which energy is scattered out of the wave by an obstacle of radius "a" to the total energy of the incident wave. The scattered energy is equal to the energy being carried away by the scattered wave across a spherical surface of radius "b" > "a". Love[33] gives this scattered energy as

$$E_{\text{scattered}} = \iint_A \left\{ \sigma_{xr} \frac{\partial u_x}{\partial t} + \sigma_{yr} \frac{\partial u_y}{\partial t} + \sigma_{zr} \frac{\partial u_z}{\partial t} \right\}_{\text{scattered}} dA \ , \qquad \text{(A29)}$$

where $\sigma_{xr}$, $\sigma_{yr}$, and $\sigma_{zr}$ are the stress components acting in the three rectangular axes on a surface normal to the radius vector $\vec{r}$, and the u's are displacements. Both the $\sigma$'s and the u's are usually complex, so care must be exercised to assure that the final expression for the scattered energy is real. Assuming a time dependence of $e^{i\omega t}$ for the displacement potentials and using the spherical symmetry of the scattered wave, Eq. (A29) can be rewritten in spherical coordinates as

$$E_{\text{scattered}} = \frac{i\omega}{2} \int_0^{\pi} \left\{ \left[ \sigma_{rr} u_r^* + \sigma_{\theta r} u_\theta^* + \sigma_{zr} u_z^* \right] \right.$$
$$\left. - \left[ \sigma_{rr}^* u_r + \sigma_{\theta r}^* u_\theta + \sigma_{zr}^* u_z \right] \right\}_{\substack{r=b \\ \text{scattered} \\ \text{wave}}} 2\pi b^2 \sin\theta d\theta \ , \qquad \text{(A30)}$$

where all the terms are defined by Eq. (A26) and the asterisk denotes the complex conjugate. The integral in this equation can be evaluated by the substitution of Eqs. (A23) and (A24) and using the identity

$$\int_0^{\pi} (\Omega f)\, g \sin\theta d\theta = \int_0^{\pi} f(\Omega g) \sin\theta d\theta = -\int_0^{\pi} \frac{\partial f}{\partial \theta} \frac{\partial g}{\partial \theta} \sin\theta d\theta \qquad \text{(A31)}$$

to determine the recursion relations and the orthogonality of the Bessel functions and the Legendre polynomials. Equation (A31) is valid for any two arbitrary functions f and g and the energy lost from the incident wave due to scattering from the spherical scatterer is

$$E_{\text{scattered}} = 4\pi\rho_1\omega^3 \sum_{m=0}^{\infty} \frac{1}{2m+1}\left[\frac{1}{k_1}|A_m|^2 + \frac{m(m+1)}{K_1}|B_m|^2\right] , \qquad \text{(A32)}$$

where $A_m$ and $B_m$ are the magnitudes of the scattered wave potentials and must be evaluated at the scattering surface by the boundary conditions.

The total energy of the wave is determined by calculating the energy in the incident plane wave that is being transported through a unit area normal to the propagation direction. The displacement of a plane wave of unit amplitude traveling in the positive x-direction can be written as

$$\vec{u} = \hat{z}\, e^{i(\omega t - K_1 z)} . \qquad \text{(A33)}$$

From elasticity theory, the stress can be calculated from the relation

$$\sigma_{ij} = \lambda(\nabla\cdot\vec{u})\ \delta_{ij} + \mu\left(\frac{\partial u_i}{\partial x_j} + \frac{\partial u_j}{\partial x_i}\right) , \qquad \text{(A34)}$$

where

$$\delta_{ij} = \begin{cases} 1 & i=j \\ 0 & i\neq j \end{cases} .$$

For the wave described, $\sigma_{ij} = 0$ for all ij except

$$\sigma_{zz} = - i \frac{\rho_1}{K_1} e^{i(\omega t - K_1 z)} \quad . \tag{A35}$$

The energy flux through a unit area is then given by

$$E_{inc} = \frac{i\omega}{2} \left\{ (\sigma_{xz} u_x^* + \sigma_{yz} u_y^* + \sigma_{zz} u_z^*) - (\sigma_{xz}^* u_x + \sigma_{yz}^* u_y + \sigma_{zz}^* u_z) \right\} = \frac{\rho_1 \omega^3}{K_1} \quad . \tag{A36}$$

The scattering cross section is defined as

$$\gamma = \frac{E_{scattered}}{E_{total}} \quad . \tag{A37}$$

Therefore, for a transverse plane wave encountering a liquid-filled spherical scatterer

$$\gamma_{shear} = 4\pi \sum_{m=0}^{\infty} \frac{1}{2m+1} \left[ \frac{K_1}{k_1} |A_m|^2 + m(m+1) |B_m|^2 \right] . \tag{A38}$$

A similar calculation for the problem of a plane compressional wave striking the liquid-filled cavity yields the similar expression

$$\gamma_{comp} = 4\pi \sum_{m=0}^{\infty} \frac{1}{2m+1} \left[ |A_m|^2 + m(m+1) \frac{k_1}{K_1} |B_m|^2 \right] . \tag{A39}$$

The scattering cross section times the square of the frequency ($\gamma \nu^2$) as a function of the circumference to wavelength of the scatterer has been solved using the computer program SCTTER given in Appendix B and the results shown in Figures 13-15 of the text.

# APPENDIX B

## COMPUTER PROGRAMS

## PROGRAM SOLID

```
ATTACH(GRAFIX)
LIBRARY(GRAFIX)
FORTRAN.
LGO(LC=3000)
      PROGRAM SOLIDWF(INPUT,OUTPUT,TAPE5=INPUT,TAPE6=OUTPUT,TAPE99)
      IMPLICIT COMPLEX(A,F,G),REAL(K)
      COMPLEX BETA
      DIMENSION G(4,5), A(4,5), F(4), KK(4), ENG(8), CP(8,1000)
      COMMON N, NN, G, F
      CALL PLOTS
      CALL PLOT(0.,2.,-3)
      NNX=0
      READ(5,100)NNN,NP
  100 FORMAT (2I2)
  101 READ(5,102)C0,CR,CL,CT,RHC0,RHC,CHI0,DCHI,CHIF
  102 FORMAT(4F5.0,2F7.4,3F8.4)
      XI=DCHI/5.
      XJ=DCHI*8.
      PI=3.141592654
      R=RHO/RHO0
      K0=1./C0
      KR=1./CR
      KL=1./CL
      KT=1./CT
      LL=IFIX((CHIF-CHI0)/DCHI+.01)
      CHI0=CHI0*PI/180.
      DCHI=DCHI*PI/180.
      CHIF=CHIF*PI/180.
      CHI=CHI0
      DO117IL=1,LL
      CHEK1=0.
      CHEK2=0.
      IF(CHI)104,105,104
  104 IF(IL-1)106,106,105
  105 CHI=CHI+DCHI
  106 BETA=K0*SIN(CHI)
      A0=K0*COS(CHI)
      AR=CONJG(CSQRT(KR**2-BETA**2))
      AL=CONJG(CSQRT(KL**2-BETA**2))
      AT=CONJG(CSQRT(KT**2-BETA**2))
      N=4
      NN=N+1
      DO 107 I=1,N
      DO 107 M=1,NN
  107 G(I,M)=0.
      G(1,1)=1.
      G(1,2)=-BETA/A0
      G(1,3)=AL/A0
      G(1,4)=-G(1,2)
      G(1,5)=1.
      G(2,1)=1.
      G(2,2)=AR/BETA
      G(2,3)=-1.
      G(2,4)=AT/BETA
      G(2,5)=-1.
      G(3,1)=-(1.-2.*(BETA**2/KR**2))
      G(3,2)=2.*BETA*AR/KR**2
```

```
      G(3,3)=(1.-2.*(BETA**2/KT**2))*R
      G(3,4)=2.*R*BETA*AT/KT**2
      G(3,5)=-G(3,1)
      G(4,1)=2.*A0*BETA/KR**2
      G(4,2)=-G(3,1)
      G(4,3)=AL*G(3,4)/AT
      G(4,4)=-G(3,3)
      G(4,5)=G(4,1)
      CALL SOLN
      DO 108 IJ=1,4
  108 KK(IJ)=CABS(F(IJ))**2
      ENG(1)=KK(1)
      ENG(2)=REAL((AR/A0)*KK(2))
      ENG(3)=REAL(R*(AL/A0)*KK(3))
      ENG(4)=REAL(R*(AT/A0)*KK(4))
      DO 200 IJ=1,4
      CHEK1=CHEK1+ENG(IJ)
  200 CONTINUE
      DO 109 I=1,N
      DO 109 M=1,NN
  109 G(I,M)=0.
      G(1,1)=A0/BETA
      G(1,2)=-1.
      G(1,3)=AL/BETA
      G(1,4)=1.
      G(1,5)=1.
      G(2,1)=BETA/AR
      G(2,2)=1.
      G(2,3)=-G(2,1)
      G(2,4)=AT/AR
      G(2,5)=1.
      G(3,1)=-(1.-2.*(BETA**2/KR**2))
      G(3,2)=2.*BETA*AR/KR**2
      G(3,3)=R*(1.-2.*(BETA**2/KT**2))
      G(3,4)=2.*R*BETA*AT/KT**2
      G(3,5)=G(3,2)
      G(4,1)=2.*A0*BETA/KR**2
      G(4,2)=-G(3,1)
      G(4,3)=AL*G(3,4)/AT
      G(4,4)=-G(3,3)
      G(4,5)=G(3,1)
      CALL SOLN
      DO 110 IJ=1,4
  110 KK(IJ)=CABS(F(IJ))**2
      ENG(5)=REAL((A0/AR)*KK(1))
      ENG(6)=KK(2)
      ENG(7)=REAL(R*(AL/AR)*KK(3))
      ENG(8)=REAL(R*(AT/AR) *KK(4))
      DO 201 IJ=5,8
      CHEK2=CHEK2 + ENG(IJ)
  201 CONTINUE
      THETA=CHI * 180./PI
      IF(IL-1)111,111,115
  111 WRITE(6,112)
  112 FORMAT(1H1)
      WRITE (6,113) C0, CR, CL, CT, RHO, RHO0
  113 FORMAT (3X, 5HC0 = , F5.0, 3X, 5HCR = , F5.0, 3X, 5HCL = ,
     $ F5.0, 3X, 5HCT = , F5.0, 3X, 6HRHO = , F4.2, 3X, 7HRHO0 = ,
     $ F4.2, /)
```

```
      WRITE (6, 114)
114   FORMAT (8X, 33H---COMPRESSIONAL WAVE INCIDENT---, 6X,
     $33H----TRANSVERSE WAVE INCIDENT-----, /, 1X, 5HTHETA,
     $3X, 2HA2, 5X, 2HB2, 5X, 2HA3, 5X, 2HB3, 4X, 5HCHEK1,  6X,
     $2HA2, 5X, 2HB2, 5X, 2HA3, 5X, 2HB3, 4X, 5HCHEK2)
C     A3 AND B3 ARE THE TRANSMITTED COMPRESSIONAL AND TRANSVERSE
C     WAVE ENERGIES RESPECTIVELY.
115   WRITE (6,116) THETA, (ENG(NM), NM=1,4), CHEK1,  (ENG(NM), NM=5,8),
     $CHEK2
116   FORMAT (1X, F5.2, 4(2X, F5.3), 2X, F5.3, 4X, 4(2X, F5.3), 2X,
     $F5.3)
      DO 10 IP=1,8
      CP(IP,IL) = ENG(IP) * 10.
   10 CONTINUE
117   CONTINUE
      IP = 0
      DO 55 J=1,2
      YP=6.
      DO 45 IQ=1,4
      RI=IQ
      IR=IQ-1
      IF(IR.EQ.3) IR=5
      IP = IP+1
      XN = XI
      CALL PLOT(XN,CP(IP,1),3)
      DO 35 IL=2,LL
      XN = XN+XI
      CALL PLOT(XN,CP(IP,IL),2)
   35 CONTINUE
      XN = XJ/4.*RI
      IS=IQ*10
      YP=YP-.25
      YS=YP+.07
      CALL SYMBOL(2.,YS,.14,IR,0.,-1)
      CALL SYMBOL(2.17,YP,.14,1H-,0.,1)
      DO 40 IL=IS,LL,40
      CALL SYMBOL(XN,CP(IP,IL),.14,IR,0.,-1)
      XN = XN+XJ
   40 CONTINUE
   45 CONTINUE
      CALL PLOT (18., 0., 3)
      CALL PLOT (0., 0., 2)
      CALL PLOT (0., 10., 2)
      CALL PLOT(18.,10.,2)
      CALL PLOT (18., 0., 2)
      XP=16.
      YP=0.1
      YZ=0.
      DO 451 L=1,8
      CALL PLOT (XP, YP, 3)
      CALL PLOT (XP, YZ, 2)
      XP=XP - 2.
451   CONTINUE
      YP=1.
      XP=0.1
      XZ=0.
      DO 452  L=1,9
      CALL PLOT (XP, YP, 3)
```

```
      CALL PLOT (XZ, YP, 2)
      YP=YP+1.
452   CONTINUE
      YP=-0.07
      XP=-.42
      YN=0.
      DO 453 L=1,11
      CALL NUMBER (XP,YP,.14,YN,0.,1)
      YN=YN+.1
      YP=YP+1.
453   CONTINUE
      CALL SYMBOL (-.65,4.1,.14,15HRELATIVE ENERGY,90.,15)
      IF (J .EQ. 1)  XP=6.36
      IF (J .EQ. 2)  XP=6.54
      IF(NP.EQ.1) GO TO 230
      CALL SYMBOL (1.7,10.4,.21,81HRELATIVE ENERGY DISTRIBUTION OF ACOUS
     $TIC WAVE INCIDENT ON PERMAFROST-ICE BOUNDARY,0.,81)
      IF (NNX .EQ. 0)  CALL SYMBOL (XP+.06, 10.10, .14,
     $15HOTTAWA SAND-ICE,0.,15)
      IF (NNX .EQ. 1)  CALL SYMBOL (XP,10.10,.14,16HHANOVER SILT-ICE,
     $ 0.,16)
      IF (NNX .EQ. 2)  CALL SYMBOL(XP-.06,10.1,.14,17HGOODRICH CLAY-ICE,
     $0.,17)
      GO TO 240
  230 CONTINUE
      CALL SYMBOL(0.8,10.4,.21,91HRELATIVE ENERGY DISTRIBUTION OF ACCUST
     $IC WAVE INCIDENT ON BOUNDARY OF TWO PERMAFROST LAYERS,0.,91)
      CALL SYMBOL(XP-.54,10.1,.14,25HOTTAWA SAND-GOODRICH CLAY,0.,25)
  240 CONTINUE
      IF (J .EQ. 2)  GO TO 454
      CALL SYMBOL(999.,999.,.14,30H (COMPRESSIONAL WAVE INCIDENT),0.,30)
      GO TO 455
454   CONTINUE
      CALL SYMBOL (999.,999.,.14,27H (TRANSVERSE WAVE INCIDENT),0.,27)
455   CONTINUE
      CALL SYMBOL(2.35,5.75,.14,23HREFLECTED COMPRESSIONAL,0.,23)
      CALL SYMBOL (2.35,5.5,.14,15HREFLECTED SHEAR,0.,15)
      CALL SYMBOL (2.35,5.25,.14,25HTRANSMITTED COMPRESSIONAL,0.,25)
      CALL SYMBOL (2.35,5.0,.14,17HTRANSMITTED SHEAR,0.,17)
      XN=10.
      XP=1.9
      YP=-0.24
      CALL NUMBER (-.04,YP,.14,0.,0.,-1)
      DO 456 L=1,9
      CALL NUMBER (XP,YP,.14,XN,0.,-1)
      XN=XN+10.
      XP=XP+2.
456   CONTINUE
      CALL SYMBOL (7.58,-0.48,.14,24HINCIDENT ANGLE (DEGREES), 0.,24)
      CALL PLOT(24.,0.,-3)
   55 CONTINUE
      NNX = NNX + 1
      IF (NNX - NNN)  101, 118, 118
118   CONTINUE
      X=0.
      Y=0.
      DO 130 L=1,4
```

```
      LP=L
      IF(LP.EQ.4) LP=5
      DO 120 LX=1,11
      CALL SYMBOL(X,Y,.14,LP,0.,-1)
      Y=Y+1.
  120 CONTINUE
      X=X+1.
      Y=0.
  130 CONTINUE
      CALL PLOT(0.,0.,999)
      STOP
      END
      SUBROUTINE SOLN
      IMPLICIT COMPLEX (A, F, G), REAL (K)
      COMPLEX SUMPR
      DIMENSION G(4,5), A(4,5), F(4)
      COMMON N, NN, G, F
C     THE AUXILLARY MATRIX FOR THE SOLUTION OF THE MATRIX BY THE CROUT
C     METHOD FOLLOWS.
      DO 104 I=1,N
104   A(I,1)=G(I,1)
      DO 111 I=2,N
      DO 111 M=2,NN
      A(1,M)=G(1,M)/A(1,1)
      SUMPR=CMPLX(0.,0.)
      IF(I-M) 105, 107, 109
105   II=I-1
      DO 106 MM=1,II
106   SUMPR=SUMPR+A(I,MM)*A(MM,M)
      A(I,M)=(G(I,M)-SUMPR)/A(I,I)
      GO TO 111
107   II=I-1
      DO 108 IJ=1,II
108   SUMPR=SUMPR+A(I,IJ)*A(IJ,I)
      A(I,I)=G(I,I)-SUMPR
      GO TO 111
109   MM=M-1
      DO 110 IJ=1,MM
110   SUMPR=SUMPR+A(I,IJ)*A(IJ,M)
      A(I,M)=G(I,M)-SUMPR
111   CONTINUE
C     THE FOLLOWING DETERMINES THE FINAL MATRIX BY THE CROUT METHOD-
C     FOR THE PROBLEM CONSIDERED.
      F(N)=A(N,NN)
      MM=N-1
      DO 115 M=1,MM
      L=N-M
      ML=L+1
      SUMPR=CMPLX(0.,0.)
112   IF(N-ML)114, 113, 113
113   SUMPR=SUMPR+A(L,ML)*F(ML)
      ML=ML+1
      GO TO 112
114   F(L)=A(L,NN)-SUMPR
115   CONTINUE
      RETURN
      END
```

## PROGRAM TRNTION

```
ATTACH(GRAFIX)
LIBRARY(GRAFIX)
FORTRAN.
LGO(LC=6000)
      PROGRAM TRNTICN(INPUT,CUTPUT,TAPE5=INPUT,TAPE6=OUTPUT)
C     THIS PROGRAM CALCULATES THE REFLECTION COEFFICIENT FROM A
C     TRANSITICN LAYER BETWEEN TWO ELASTIC MEDIA.
      IMPLICIT REAL(K,N)
      COMPLEX I,GM1,GP1,A2
      DIMENSION HOLD(2),X(500),YC(500),YT(500)
      CALL PLOTS
      CALL PLOT(0.,1.,-3)
  116 CONTINUE
  100 READ(5,101)C0,CR,CC,CS,RHO0,RHO2,N,MNX
  101 FORMAT(4F5.0,2F5.3,F3.0,I3)
      IF(EOF,5) 300,102
  102  CONTINUE
      IF(MNX.EQ.0) GO TC 1
      PS=40.
      PL=.025
      GO TO 2
    1 CONTINUE
      PS=20.
      PL=.05
    2 CONTINUE
      NT=0.
      I=(0.,1.)
      K0H=0.
      DO 114 L=1,500
      K0H=K0H+.02
      NT=NT+1.
  104 KRH=K0H*C0/CR
      KCH=K0H*C0/CC
      KSH=K0H*C0/CS
      IF(N)105,105,106
  105 ALPH=0.
      ALPT=0.
      GO TO 107
  106 XN=1./N
      ALPH=(CC/C0)**XN-1.
      ALPT=(CS/CR)**XN-1.
C     KLH AND KTH DEFINE THE TRANSITION
  107 KLH=K0H/(1.+ALPH)**N
      KTH=KRH/(1.+ALPT)**N
      NM1=N-1.
C     FIRST CALCULATE FCR COMPRESSIONAL INCIDENT
      P=(1.-(N-1.)*ALPH)/(1.+ALPH)**NM1
      Q=(1.-(N-1.)*ALPH)**2
      R=(2.*ALPH*N/K0H)*(1.-0.5*(N-1.)*ALPH)*((1.+ALPH)**N)
      X1=(RHO2/RHO0)*(K0H/KCH)*P-Q+R*TAN(KLH)
      X2=R+(Q-(K0H/KCH)*P)*TAN(KLH)
      X3=Q-R*TAN(KLH)
      X4=(K0H/KCH)*P*TAN(KLH)
      Y1=(RHO2/RHO0)*(K0H/KCH)*P+Q-R*TAN(KLH)
      Y2=R+(Q+(K0H/KCH)*P)*TAN(KLH)
      GM1=(X1+I*X2)/(X3+I*X4)
      GP1=(Y1+I*Y2)/(X3+I*X4)
```

```
      A2=(GM1-2.*I*N*ALPH/KOH)/(GP1-2.*I*N*ALPH/KOH)
      HOLD(1)=CABS(A2)
      Z=(RHO2*CC)/(RHO0*C0)
      TEST=(1.-Z)/(1.+Z)
      IF(HOLD(1)-TEST)201,201,200
  200 HOLD(1)=TEST
  201 CONTINUE
      ENGC=HOLC(1)**2
C     NOW CALCULATE FOR TRANSVERSE WAVE INCIDENT
      P=(1.-(N-1.)*ALPT)/(1.+ALPT)**NM1
      Q=(1.-(N-1.)*ALPT)**2
      R=(2.*ALPT*N/KRH)*(1.-0.5*(N-1.)*ALPT)*((1.+ALPT)**N)
      X1=(RHO2/RHO0)*(KRH/KSH)*P-Q+R*TAN(KTH)
      X2=R+(Q-(KRH/KSH)*P)*TAN(KTH)
      X3=Q-R*TAN(KTH)
      X4=(KRH/KSH)*P*TAN(KTH)
      Y1=(RHO2/RHO0)*(KRH/KSH)*P+Q-R*TAN(KTH)
      Y2=R+(Q+(KRH/KSH)*P)*TAN(KTH)
      GM1=(X1+I*X2)/(X3+I*X4)
      GP1=(Y1+I*Y2)/(X3+I*X4)
      A2=(GM1-2.*I*N*ALPT/KRH)/(GP1-2.*I*N*ALPT/KRH)
      HOLD(2)=CABS(A2)
      Z=(RHO2*CS)/(RHO0*CR)
      TEST=(1.-Z)/(1.+Z)
      IF(HOLD(2)-TEST)203,203,202
  202 HOLD(2)=TEST
  203 CONTINUE
      ENGT=HOLD(2)**2
      IF(NT-1.)108,108,115
  108 CONTINUE
      IF(MNX.EQ.0) WRITE(6,111)
      IF(MNX.EC.1) WRITE(6,121)
      IF(MNX.EQ.2) WRITE(6,131)
  111 FORMAT(1H1,16X,15HOTTAWA SAND-ICE)
  121 FORMAT(1H1,15X,16HHANCVER SILT-ICE)
  131 FORMAT(1H1,15X,17HGOODRICH CLAY-ICE)
      WRITE(6,109) N
  109 FORMAT(10X,27HTRANSITICN OF FORM (1+AX)**
     1,F2.0,/,12X,17H..COMPRESSICNAL..,3X,17H...TRANSVERSE....)
      WRITE(6,112)
  112 FORMAT(5X,3HKOH,4X,7HCMP AMP,3X,7HCMP ENG,3X,7HSHR AMP,3X,7HSHR EN
     1G)
  115 WRITE(6,113)KOH,HCLD(1),ENGC,HOLD(2),ENGT
  113 FORMAT(1X,F8.3,4(3X,F7.4))
      X(L)=KOH
      YC(L)=ENGC*PS
      YT(L)=ENGT*PS
  114 CONTINUE
      CALL PLOT(X(1),YC(1),3)
      DO 10 J=2,500
      CALL PLOT(X(J),YC(J),2)
   10  CONTINUE
      DO 15 J=20,500,20
      CALL SYMBOL(X(J),YC(J),.136,0,0.,-1)
   15 CONTINUE
      CALL PLOT(X(1),YT(1),3)
      DO 27 J=2,500
```

```
      CALL PLOT(X(J),YT(J),2)
27    CONTINUE
      DO 46 J=10,490,20
      CALL SYMBOL(X(J),YT(J),.136,1,0.,-1)
46    CONTINUE
      CALL PLOT(10.,0.,3)
       CALL PLOT(0.,0.,2)
      CALL PLOT(0.,8.,2)
      CALL PLOT(10.,8.,2)
      CALL PLOT(10.,0.,2)
      XP=9.
       YP=0.1
      YZ=0.
      DO 48 J=1,9
      CALL PLOT(XP,YP,3)
      CALL PLOT(XP,YZ,2)
       XP=XP-1.
48    CONTINUE
      YP=1.
      XP=0.1
      XZ=0.
      DO 60 J=1,7
       CALL PLOT(XP,YP,3)
      CALL PLOT(XZ,YP,2)
      YP=YP+1.
   60 CONTINUE
      YP=-0.07
      XP=-.7
      YN=0.
       DO 65 J=1,9
      CALL NUMBER(XP,YP,.14,YN,0.,3)
      YN=YN+PL
      YP=YP+1.
65    CONTINUE
      CALL SYMBOL(-.89,3.1,.14,15HRELATIVE ENERGY,90.,15)
      CALL SYMBOL(2.66,8.40,.21,25HTRANSITION OF FORM (1+AX),0.,25)
      CALL NUMBER(999.,8.56,.14,N,0.,-1)
      IF(MNX.EQ.0) CALL SYMBOL(4.10,8.1,.14,15HOTTAWA SAND-ICE  ,0.,15)
      IF(MNX.EQ.1) CALL SYMBOL(4.04,8.1,.14,16HHANOVER SILT-ICE ,0.,16)
      IF(MNX.EQ.2) CALL SYMBOL(3.98,8.1,.14,17HGOODRICH CLAY-ICE,0.,17)
      CALL SYMBOL(6.0,7.0,.136,0,0.,-1)
      CALL SYMBOL(6.17,6.93,.14,1H-,0.,1)
      CALL SYMBOL(6.35,6.93,.14,22HCOMPRESSIONAL INCIDENT,0.,22)
      CALL SYMBOL(6.0,6.75,.136,1,0.,-1)
      CALL SYMBOL(6.17,6.68,.14,1H-,0.,1)
      CALL SYMBOL(6.35,6.68,.14,14HSHEAR INCIDENT,0.,14)
      XN=0.
      XP=-.04
      YP=-0.24
      DO 75 J=1,10
      CALL NUMBER(XP,YP,.14,XN,0.,-1)
      XN=XN+1.
      XP=XP+1.
   75 CONTINUE
      CALL NUMBER(9.9,YP,.14,XN,0.,-1)
      CALL SYMBOL(4.82,-.48,.14,1HK,0.,1)
      CALL SYMBOL(4.944,-.536,.112,1H0,0.,1)
```

```
      CALL SYMBOL(5.064,-.48,.14,1HH,0.,1)
      CALL PLOT(14.,0.,-3)
      GO TO 116
  300 CONTINUE
      CALL PLOT(0.,0.,999)
      STOP
      END
```

## PROGRAM SCATER

```
FORTRAN.
LGO.
      PROGRAM SCATER(INPUT,OUTPUT,TAPE5=INPUT,TAPE6=OUTPUT)
      IMPLICIT REAL (J,K)
      COMMON KL1,KS1,KL2,KS2,RHO1,RHO2,SIM,CIM,GAMMA,AK,J(400),NMAX,
     1Y(400),CL1,CS1,CL2,CS2
C     THIS PROGRAM CALCULATES THE SCATTERING CROSS SECTION TIMES THE
C     FREQUENCY SQUARED FOR A SHEAR AND COMPRESSIONAL PLANE WAVE
C     IMPINGING ON AN ELASTIC SPHERE EMBEDDED IN AN ELASTIC MEDIUM.
C     THE VALUE IS CALCULATED AS A FUNCTION OF THE DIMENSIONLESS
C     PARAMETER KA WHERE K=2.*PI*FREQUENCY/VELOCITY AND A IS THE SPHERE
C     RADIUS.  THE CALCULATION IS MADE IN THE C.G.S. SYSTEM. THE
C     SCATTERING CROSS SECTION HAS UNITS OF DB-CM**2.  CS1 AND CS2 ARE
C     THE SHEAR AND CL1 AND CL2 ARE THE COMPRESSIONAL VELOCITIES IN THE
C     MEDIUM AND SCATTERER RESPECTIVELY.  RHO1 AND RHO2 ARE THE
C     RESPECTIVE DENSITIES.
      WRITE(6,97)
   97 FORMAT(1H1,45X,12HHANCVER SILT)
      READ(5,98)CL1,CS1,CL2,CS2,RHO1,RHO2
   98 FORMAT(4F8.0,2F6.3)
      CL1=CL1*100.
      CS1=CS1*100.
      CL2=CL2*100.
      CS2=CS2*100.
      WRITE(6,99)
   99 FORMAT(5X,2HKA,7X,11HGAMMA,SHEAR,7X,10HGAMMA,COMP)
  100 READ(5,101)KA
  101 FORMAT(F7.2)
      IF(EOF,5)104,102
  102 CONTINUE
C     FIRST THE SHEAR SCATTERING IS CALCULATED
      KS1=KA
      KL1=KS1*CS1/CL1
      KS2=KS1*CS1/CS2
      KL2=KS1*CS1/CL2
      SIM=CS1
C     IF CIM=0., THEN A SHEAR WAVE IS INCIDENT.
      CIM=0.
      CALL SOLN
      GAMMAS=GAMMA
C     GAMMAS IS THE SHEAR SCATTERING CROSS SECTION * FREQ**2.
C     NOW CALCULATE THE COMPRESSIONAL SCATTERING CROSS SECTION.
      KL1=KA
      KS1=KL1*CL1/CS1
      KL2=KL1*CL1/CL2
      KS2=KL1*CL1/CS2
```

```
C       IF SIM=0., THEN A COMPRESSIONAL WAVE IS INCIDENT
        SIM=0.
        CIM=CL1
        CALL SOLN
        GAMMAC=GAMMA
C       GAMMAC IS THE COMPRESSIONAL SCATTERING CROSS SECTION*FREQ**2
        WRITE(6,103)KA,GAMMAS,GAMMAC
  103   FORMAT(2X,F7.2,2(5X,E13.4))
        GO TO 100
  104   CONTINUE
        END
        SUBROUTINE SOLN
        IMPLICIT REAL(J,K)
        COMPLEX A,F,G,I,SUMPR
        DIMENSION J1(400),J2(400),J3(400),J4(400),Y1(400),Y2(400),G(4,5),
       1A(4,5),F(4),KK(4)
        COMMON KL1,KS1,KL2,KS2,RHO1,RHO2,SIM,CIM,GAMMA,AK,J(400),NMAX,
       1Y(400),CL1,CS1,CL2,CS2
C       THIS ROUTINE SOLVES THE BOUNDARY CONDITIONS FOR THE AMPLITUDES OF
C       THE SCATTERED WAVE WHICH ARE USED TO CALCULATE THE SCATTERING
C       CROSS SECTIONS.
        I=(0.,1.)
        PI=3.141592654
        CALL UPRLIM
        NM=NMAX+1
        AK=KL1
        CALL SPHBES
        DO 100 L=1,NM
  100   J1(L)=J(L)
        AK=KS1
        CALL SPHBES
        DO 101 L=1,NM
  101   J2(L)=J(L)
        AK=KL2
        CALL SPHBES
        DO 102 L=1,NM
  102   J3(L)=J(L)
        AK=KS2
        CALL SPHBES
        DO 103 L=1,NM
  103   J4(L)=J(L)
        NM=NMAX+2
        AK=KL1
        CALL SPHNEU
        DO 111 M=1,NM
  111   Y1(M)=Y(M)
        AK=KS1
        CALL SPHNEU
        DO 112 M=1,NM
  112   Y2(M)=Y(M)
        GAMMA =0.
        DO 127 M=1,NMAX
```

```
      N1=4
      N2=N1+1
      DO 113 NX=1,N1
      DO 113 NY=1,N2
  113 G(NX,NY)=0.
      G(1,1)=-(M*J1(M)-KL1*J1(M+1))+I*(M*Y1(M)-KL1*Y1(M+1))
      G(1,2)=(M*(M+1)*J2(M))-I*(M*(M+1)*Y2(M))
      G(1,3)=(M*J3(M)-KL2*J3(M+1))
      G(1,4)=-M*(M+1)*J4(M)
      G(1,5)=CIM*(M*J1(M)-KL1*J1(M+1))-SIM*(M*(M+1)*J2(M))
      G(2,1)=-J1(M)+I*Y1(M)
      G(2,2)=((M+1)*J2(M)-KS1*J2(M+1))-I*((M+1)*Y2(M)-KS1*Y2(M+1))
      G(2,3)=J3(M)
      G(2,4)=-((M+1)*J4(M)-KS2*J4(M+1))
      G(2,5)=CIM*J1(M)-SIM*((M+1)*J2(M)-KS1*J2(M+1))
      G(3,1)=-((0.5*KS1**2-M*(M-1))*J1(M)-2.*KL1*J1(M+1))
     1+I*((0.5*KS1**2-M*(M-1))*Y1(M)-2.*KL1*Y1(M+1))
      G(3,2)=-M*(M+1)*((M-1)*J2(M)-KS1*J2(M+1))+I*M*(M+1)*((M-1)*Y2(M)
     1-KS1*Y2(M+1))
      KS=KS1**2/KS2**2
      R=RHO2/RHO1
      G(3,3)=R*KS*((0.5*KS2**2-M*(M-1))*J3(M)-2.*KL2*J3(M+1))
      G(3,4)=R*KS*M*(M+1)*((M-1)*J4(M)-KS2*J4(M+1))
      G(3,5)=CIM*((0.5*KS1**2-M*(M-1))*J1(M)-2.*KL1*J1(M+1))
     1+SIM*(M*(M+1)*((M-1)*J2(M)-KS1*J2(M+1)))
      G(4,1)=-((M-1)*J1(M)-KL1*J1(M+1))+I*((M-1)*Y1(M)-KL1*Y1(M+1))
      G(4,2)=-((1.-M**2+0.5*KS1**2)*J2(M)-KS1*J2(M+1))+I*((1-M**2
     1+0.5*KS1**2)*Y2(M)-KS1*Y2(M+1))
      G(4,3)=R*KS*((M-1)*J3(M)-KL2*J3(M+1))
      G(4,4)=R*KS*((1.-M**2+0.5*KS2**2)*J4(M)-KS2*J4(M+1))
      G(4,5)=CIM*((M-1)*J1(M)-KL1*J1(M+1))+SIM*((1.-M**2+0.5*KS1**2)
     1*J4(M)-KS2*J4(M+1))
C     THE AUXILLARY MATRIX FOR THE SOLUTION BY THE CROUT METHOD FOLLOWS
      DO 114 MX=1,N1
  114 A(MX,1)=G(MX,1)
      DO 121 NX=2,N1
      DO 121 MX=2,N2
      A(1,MX)=G(1,MX)/A(1,1)
      SUMPR=CMPLX(0.,0.)
      IF(NX-MX)115,117,119
  115 LL=NX-1
      DO 116 MM=1,LL
  116 SUMPR=SUMPR+A(NX,MM)*A(MM,MX)
      A(NX,MX)=(G(NX,MX)-SUMPR)/A(NX,NX)
      GO TO 121
  117 LL=NX-1
      DO 118 MM=1,LL
  118 SUMPR=SUMPR+A(NX,MM)*A(MM,NX)
      A(NX,NX)=G(NX,NX)-SUMPR
      GO TO 121
  119 LL=MX-1
      DO 120 MM=1,LL
  120 SUMPR=SUMPR+A(NX,MM)*A(MM,MX)
      A(NX,MX)=G(NX,MX)-SUMPR
  121 CONTINUE
C     THE FOLLOWING DETERMINES THE FINAL MATRIX BY THE CROUT METHOD
      F(N1)=A(N1,N2)
      LL=N1-1
```

```
      DO 125 MX=1,LL
      L=N1-MX
      ML=L+1
      SUMPR=CMPLX(0.,0.)
  122 IF(N1-ML)124,123,123
  123 SUMPR=SUMPR+A(L,ML)*F(ML)
      ML=ML+1
      GO TO 122
  124 F(L)=A(L,N2)-SUMPR
  125 CONTINUE
      DO 126 L=1,N1
  126 KK(L)=F(L)*CONJG(F(L))
      GAMMA=GAMMA+(SIM/FI)*(2*M+1)*((KS1/KL1)*KK(1)+M*(M+1)*KK(2))/CS1
     1+(CIM/PI)*(2*M+1)*(KK(1)+(KL1/KS1)*M*(M+1)*KK(2))/CL1
  127 CONTINUE
      GAMMA=8.686*GAMMA
      RETURN
      END
      SUBROUTINE UPRLIM
      IMPLICIT REAL (J,K)
      DIMENSION NN(4)
      COMMON KL1,KS1,KL2,KS2,RHO1,RHO2,SIM,CIM,GAMMA,AK,J(400),NMAX,
     1Y(400),CL1,CS1,CL2,CS2
C     THIS SUBROUTINE SETS THE UPPER LIMIT SUCH THAT ALL SPHERICAL
C     BESSEL FUNCTIONS OF HIGHER ORDER CAN BE APPROXIMATED TO ZERO.
      DO 105 II=1,4
      GO TO (96,97,98,99),II
   96 AK=KL1
      GO TO 100
   97 AK=KS1
      GO TO 100
   98 AK=KL2
      GO TO 100
   99 AK=KS2
  100 NAK=IFIX(AK)
      N=NAK+10
      DO 101 I=N,1850,5
      L=I
      FI=FLOAT(I)
      SECA=AK/(FI+0.5)
      TACA=SQRT(1.-SECA**2)
      COSA=1./SECA
      SINA=SQRT(1.+COSA**2)
      ALP=ALOG(COSA+SQRT(COSA**2-1.))
      DELT=EXP((FI+0.5)*(TACA-ALP))/(2.*(FI+0.5)*SQRT(SINA))
      IF(DELT-1.E-27)102,102,101
  101 CONTINUE
      GO TO 107
  102 N=L
      FN=FLOAT(N)
      NP=N+1
      NT=N+2
      NU=N+10
      EXPR=EXP(1.)
      DO 103 I=NU,1890,5
      L=I
      FI=FLOAT(I)
      D=0.434294
```

```
      A1=2.*(FI-FN+1.)*D*ALOG(AK)
      A2=(2.*FI-2.*FN+1.)*D*ALOG(EXPR)
      A3=(FN+2.5)*D*ALOG(FN+2.)+(FN-1.5)*D*ALOG(FN-2.)
      A4=(FI+3.5)*D*ALOG(FI+3.)
      A5=(FI-0.5)*D*ALOG(FI-1.)
      E=A1+A2+A3-A4-A5
      IF(E+10.)104,104,103
  103 CONTINUE
      GO TO 107
  104 NN(II)=NT
  105 CONTINUE
      NMAX=MAX0(NN(1),NN(2),NN(3),NN(4))
C     NMAX IS THE UPPER LIMIT OF THE SUM IN THE SCATTERING CROSS
C     SECTION. ALL HIGHER TERMS CAN BE CONSIDERED TO BE ZERO.
  106 RETURN
  107 WRITE(6,108)AK
  108 FORMAT(26H ARG BES FTN TOO LARGE KA=,E20.8,5X,14H END EXECUTION)
      STOP
      END
      SUBROUTINE SPHBES
      IMPLICIT REAL (J,K)
      DIMENSION R(400),RJ(400)
      COMMON KL1,KS1,KL2,KS2,RHO1,RHO2,SIM,CIM,GAMMA,AK,J(400),NMAX,
     1Y(400),CL1,CS1,CL2,CS2
C      THIS ROUTINE CALCULATES THE SPHERICAL BESSEL FUNCTION (J(I)) OF
C     ARGUMENT AK TO ORDER NN.  THE SOLUTION IS VALID FOR ARGUMENTS AS
C     LOW AS 0.05.
      NDIM=400
      DO 100 I=1,400
  100 J(I)=0.
  104 NU=NMAX+10
      NT=NMAX+2
      NP=NMAX+1
      IJ=NU
      R(NU+1)=0.
      DO 105 I=1,NU
      L=I
      SJ=FLOAT(IJ)
      R(IJ)=AK/(1.+2.*SJ-AK*R(IJ+1))
      IF(R(IJ)-1.)105,105,106
  105 IJ=IJ-1
      GO TO 107
  106 IF(IJ-2)107,107,111
  107 RJ(NU+1)=R(NU)
      RJ(NU)=1.
      IJ=NU
      NUP=NU-1
      DO 108 I=1,NUP
      IJ=IJ-1
      SJ=FLOAT(IJ)
      RJ(IJ)=(1.+2.*SJ)/AK*RJ(IJ+1)-RJ(IJ+2)
  108 CONTINUE
      ALPH=(RJ(1)-AK*RJ(2))*COS(AK)+AK*SIN(AK)*RJ(1)
      DO 109 I=1,NT
  109 J(I)=RJ(I)/ALPH
  110 CONTINUE
      RETURN
```

```
  111 RJ(IJ+1)=R(IJ)
      LAM2=IJ+2
      IF(LAM2-NP)112,119,119
  112 RJ(IJ)=1.
      IJ=IJ-1
      L=L+1
      DO 113 I=L,NU
      SJ=FLOAT(IJ)
      RJ(IJ)=(1.+2.*SJ)/AK*RJ(IJ+1)-RJ(IJ+2)
  113 IJ=IJ-1
      DO 114 I=LAM2,NT
  114 RJ(I)=RJ(I-1)*R(I-1)
      ALPH=(RJ(1)-AK*RJ(2))*COS(AK)+AK*SIN(AK)*RJ(1)
      NDM=NDIM-1
      IF(NT-NDM)116,116,115
  115 NT=NDM
  116 DO 117 I=1,NT
  117 J(I)=RJ(I)/ALPH
  118 CONTINUE
      RETURN
  119 WRITE(6,120)
  120 FORMAT(25H LAMBDA+2.GE.N+1  END XEQ)
      GO TO 118
      END
      SUBROUTINE SPHNEU
      COMMON KL1,KS1,KL2,KS2,RHO1,RHO2,SIM,CIM,GAMMA,AK,J(400),NMAX,
     1Y(400),CL1,CS1,CL2,CS2
C       THIS ROUTINE CALCULATES THE SPHERICAL NEUMAN FUNCTION(Y(I))
C     OF ARGUMENT AK AND UP TO ORDER NMAX.  THE VALUES ARE CALCULATED
C     BY UPWARD RECURSION RELATIONS.
      ZERO=0.
      DO 100 I=1,400
  100 Y(I)=0.
      Y(1)=ZERO-COS(AK)/AK
      Y(2)=ZERO-COS(AK)/AK**2-SIN(AK)/AK
      NT=NMAX+2
      DO 101 I=3,NT
      AJ=FLOAT(I)-2.
      Y(I)=((2.*AJ+1.)/AK)*Y(I-1)-Y(I-2)
  101 CONTINUE
      RETURN
      END
```

## REFERENCES


1. D.F. Barnes, "Geophysical Methods for Delineating Permafrost," *Proceedings of the First International Permafrost Conference*, Publ. 1287, pp. 349-355, National Research Council, National Academy of Sciences, Washington D.C. (1963).

2. Iv. D. Zykov, "Ultrasonic Methods Used in the Study of Elastic Properties of Frozen Ground Samples," *Merzlotynye Issled.*, 5 184-198 (1966).

3. J.A.M. Hunter, "The Application of Shallow Seismic Methods to Mapping of Frozen Surficial Materials," *Proceedings of the Second International Conference on Permafrost*, pp. 527-535, National Academy of Sciences, Washington D.C. (1973).

4. L.H. Adams and R.E. Gibson, "The Elastic Properties of Certain Basic Rocks and of Their Constituent Materials," *Geophysics* 15 713-724 (1929).

5. B.S. Banthia, et al., "Ultrasonic Velocities in Rocks Subjected to Simulated Overburden Pressure and Internal Pore Pressure," *Geophysics* 30 117-121 (1965).

6. M.S. King and I. Fatt, "Ultrasonic Shear Wave Velocities in Rocks Subjected to Simulated Overburden Pressure," *Geophysics* 27 590-598 (1962).

7. R.J. Urick and W.S. Ament, "The Propagation of Sound in Composite Media," *J. Acoust. Soc. Amer.* 21 115-119 (1949).

8. M.A. Biot, "Theory of Elasticity and Consolidation for a Porous Anisotropic Solid," *J. Appl. Phys.* 26 182-185 (1955).

9. M. A. Biot, "Theory of Propagation of Elastic Waves in a Fluid-Saturated Porous Solid. I. Low Frequency Range," *J. Acoust. Soc. Amer.* 28 168-178 (1956).

10. M.A. Biot, "Theory of Propagation of Elastic Waves in a Fluid-Saturated Porous Solid. II. Higher Frequency Range," *J. Acoust. Soc. Amer.* 28 179-191 (1956).

11. M.A. Biot, "Generalized Theory of Acoustic Propagation in Porous Dissipative Media," *J. Acoust. Soc. Amer.* 34 1254-1264 (1962).

12. M.A. Biot, "Mechanics of Deformation and Acoustic Propagation in Porous Media," *J. Appl. Phys.* 33 1482-1498 (1962).

13. Tung-Ming Lee, "Method of Determining Dynamic Properties of Viscoelastic Solids Employing Forced Vibration," *J. Appl. Phys.* 34A 1524-1529 (1963).

14. C.W. Kaplar, "Laboratory Determination of the Dynamic Modulii of Frozen Soils and of Ice," *Proceedings of the First International Conference on Permafrost*, Publ. 1287, pp. 393-301, National Research Council, National Academy of Sciences, Washington, D.C. (1963).

15. A. Timur, "Velocity of Compressional Waves in Porous Media at Permafrost Temperatures," *Geophysics* 33 584-595 (1968).

16. Y. Nakano, et al., "Determination of the Acoustic Properties of Frozen Soils," Cold Regions Research Evaluation Laboratory (May 1971).

17. Y. Nakano and R. Arnold, "Acoustic Properties of Frozen Ottawa Sand," *Water Resources Research* 9 178-184 (1973).

18. Y. Nakano and N. Froula, "Sound and Shock Transmission in Frozen Soils," *Proceedings of the Second International Conference on Permafrost*, pp.359-369, National Research Council, National Academy of Sciences, Washington, D.C. (1973).

19. F. Press and M.B. Dobrin, "Seismic Wave Studies over a High Speed Surface Layer," *Geophysics* 21 (2) 285-298 (1956).

20. R.J. Donato, "Measurements on the Arrival Refracted from a Thin High Speed Layer," *Geophys. Prospec.* 13 387-404 (1965).

21. H. Lamb, "On Elastic Waves in a Plate," *Proc. R. Soc. London* A93 114-128 (1917).

22. D.D. Jackson and D.L. Anderson, "Physical Mechanisms of Seismic Wave Attenuation," *Review of Geophysics and Space Physics* 8 1-63 (1970).

23. C.F. Ying and R. Truell, "Scattering of a Plane Longitudinal Wave by a Spherical Obstacle in an Isotropically Elastic Solid," *J. Appl. Phys.* 27 1086-1096 (1956).

24. F.J. Corbato´ and J.L. Uretsky, "Generation of Spherical Bessel Functions in Digital Computers," *Assoc. Computing Machinery Journal* 6 366-375 (1959).

25. Lord Rayleigh, *Theory of Sound*, Dover Publications (1945).

26. W.M. Ewing, W.S. Jardetzky, and F. Press, *Elastic Waves in Layered Media*, McGraw-Hill, New York (1957).

27. C. Maxwell, *Scientific Papers*, Cambridge University Press, Cambridge, England (1890).

28. W. Voigt, *Ann. d. Phy.* 47 671 (1892).

29. W.P. Mason, *Physical Acoustics and Properties of Solids*, Van Nostrand, Princeton, New Jersey (1958).

30. D.R. Bland, *The Theory of Linear Viscoelasticity*, Pergammon, New York (1960).

31. H. Kolsky, *Stress Waves in Solids*, Dover, New York (1963).

32. P.M. Morse and H. Feshbach, *Methods of Theoretical Physics*, McGraw-Hill, New York (1953).

33. H. Love, *The Mathematical Theory of Elasticity*, Cambridge University Press, New York (1927).

Unclassified
Security Classification

**DOCUMENT CONTROL DATA - R&D**
*(Security classification of title, body of abstract and indexing annotation must be entered when the overall report is classified)*

| | |
|---|---|
| 1. ORIGINATING ACTIVITY (Corporate author)<br>University of Washington<br>Seattle, Washington 98195 | 2a. REPORT SECURITY CLASSIFICATION<br>Unclassified<br>2b. GROUP |

3. REPORT TITLE

FEASIBILITY OF DETERMINING SUBSURFACE PERMAFROST STRUCTURE USING ACOUSTIC PULSE ECHO TECHNIQUES

4. DESCRIPTIVE NOTES (Type of report and inclusive dates)
Final Report

5. AUTHOR(S) (Last name, first name, initial)

Bunney, Robert E.

| 6. REPORT DATE | 7a. TOTAL NO. OF PAGES | 7b. NO. OF REFS |
|---|---|---|
| April 1974 | 77 | 33 |

| | |
|---|---|
| 8a. CONTRACT OR GRANT NO.<br>DAAG17-73-C-0028<br>b. PROJECT NO.<br>c.<br>d. | 9a. ORIGINATOR'S REPORT NUMBER(S)<br>APL-UW 7318<br>9b. OTHER REPORT NO(S) (Any other numbers that may be assigned this report)<br>APL-UW 7318 |

10. AVAILABILITY/LIMITATION NOTICES

Distribution of this document is unlimited.

| 11. SUPPLEMENTARY NOTES | 12. SPONSORING MILITARY ACTIVITY |
|---|---|
| | U.S. Army Natick Laboratories<br>Natick, Massachusetts 01760 |

13. ABSTRACT

The results of controlled laboratory experiments on the acoustic properties of representative samples of permafrost are reported and the data compared with theoretical predictions. Measurements of velocity, attenuation and reflectivity were performed and evaluated with respect to the feasibility of using pulse echo techniques to analyze near (<50 ft) subsurface permafrost structure. Although acoustic pulse echo techniques appear feasible, further laboratory experiments, as well as field tests to measure the acoustic properties of permafrost in situ, are recommended.

DD FORM 1 JAN 64 1473

Unclassified
Security Classification

| 14. KEY WORDS | LINK A | | LINK B | | LINK C | |
|---|---|---|---|---|---|---|
| | ROLE | WT | ROLE | WT | ROLE | WT |
| permafrost | | | | | | |
| acoustic propagation | | | | | | |
| acoustic attenuation | | | | | | |
| acoustic reflectivity | | | | | | |

## INSTRUCTIONS

1. ORIGINATING ACTIVITY: Enter the name and address of the contractor, subcontractor, grantee, Department of Defense activity or other organization *(corporate author)* issuing the report.

2a. REPORT SECURITY CLASSIFICATION: Enter the overall security classification of the report. Indicate whether "Restricted Data" is included. Marking is to be in accordance with appropriate security regulations.

2b. GROUP: Automatic downgrading is specified in DoD Directive 5200.10 and Armed Forces Industrial Manual. Enter the group number. Also, when applicable, show that optional markings have been used for Group 3 and Group 4 as authorized.

3. REPORT TITLE: Enter the complete report title in all capital letters. Titles in all cases should be unclassified. If a meaningful title cannot be selected without classification, show title classification in all capitals in parenthesis immediately following the title.

4. DESCRIPTIVE NOTES: If appropriate, enter the type of report, e.g., interim, progress, summary, annual, or final. Give the inclusive dates when a specific reporting period is covered.

5. AUTHOR(S): Enter the name(s) of author(s) as shown on or in the report. Enter last name, first name, middle initial. If military, show rank and branch of service. The name of the principal author is an absolute minimum requirement.

6. REPORT DATE: Enter the date of the report as day, month, year; or month, year. If more than one date appears on the report, use date of publication.

7a. TOTAL NUMBER OF PAGES: The total page count should follow normal pagination procedures, i.e., enter the number of pages containing information.

7b. NUMBER OF REFERENCES: Enter the total number of references cited in the report.

8a. CONTRACT OR GRANT NUMBER: If appropriate, enter the applicable number of the contract or grant under which the report was written.

8b, 8c, & 8d. PROJECT NUMBER: Enter the appropriate military department identification, such as project number, subproject number, system numbers, task number, etc.

9a. ORIGINATOR'S REPORT NUMBER(S): Enter the official report number by which the document will be identified and controlled by the originating activity. This number must be unique to this report.

9b. OTHER REPORT NUMBER(S): If the report has been assigned any other report numbers *(either by the originator or by the sponsor)*, also enter this number(s).

10. AVAILABILITY/LIMITATION NOTICES: Enter any limitations on further dissemination of the report, other than those imposed by security classification, using standard statements such as:

(1) "Qualified requesters may obtain copies of this report from DDC."

(2) "Foreign announcement and dissemination of this report by DDC is not authorized."

(3) "U. S. Government agencies may obtain copies of this report directly from DDC. Other qualified DDC users shall request through _____."

(4) "U. S. military agencies may obtain copies of this report directly from DDC. Other qualified users shall request through _____."

(5) "All distribution of this report is controlled. Qualified DDC users shall request through _____."

If the report has been furnished to the Office of Technical Services, Department of Commerce, for sale to the public, indicate this fact and enter the price, if known.

11. SUPPLEMENTARY NOTES: Use for additional explanatory notes.

12. SPONSORING MILITARY ACTIVITY: Enter the name of the departmental project office or laboratory sponsoring *(paying for)* the research and development. Include address.

13. ABSTRACT: Enter an abstract giving a brief and factual summary of the document indicative of the report, even though it may also appear elsewhere in the body of the technical report. If additional space is required, a continuation sheet shall be attached.

It is highly desirable that the abstract of classified reports be unclassified. Each paragraph of the abstract shall end with an indication of the military security classification of the information in the paragraph, represented as *(TS)*, *(S)*, *(C)*, or *(U)*.

There is no limitation on the length of the abstract. However, the suggested length is from 150 to 225 words.

14. KEY WORDS: Key words are technically meaningful terms or short phrases that characterize a report and may be used as index entries for cataloging the report. Key words must be selected so that no security classification is required. Identifiers, such as equipment model designation, trade name, military project code name, geographic location, may be used as key words but will be followed by an indication of technical context. The assignment of links, roles, and weights is optional.


DATE
ILME
8